Recent advances in plasmonic photonic crystal fibers: design, fabrication and applications

DORA JUAN JUAN HU,[1,*] HO PUI HO[2]

[1] *Institute for Infocomm Research, Singapore*
[2] *Department of Electronic Engineering, The Chinese University of Hong Kong, Hong Kong SAR, China*
[*] *Corresponding author: jjhu@i2r.a-star.edu.sg*

Received Month Day, Year; revised Month Day, Year; accepted Month Day, Year; published Month Day Year (Doc. ID xxxxx)

The flexibility in engineering the holey structure and controlling the wave guiding properties in photonic crystal fibers (PCFs) has enabled a wide variety of PCF-based plasmonic structures and devices with attractive application potential. Metal thin films, nanowires and nanoparticles are embedded for achieving surface plasmon resonance (SPR) or localized SPR within PCF structure. This article begins with an outline of plasmonic sensing principle. This is followed by an overview on fabrication and experimental investigation of plasmonic PCFs. Reported plasmonic PCF designs are categorized based on their target application areas including optical/biochemical sensors, polarization splitters and couplers. Finally, design and fabrication considerations, as well as limitations due to structural features of PCFs, are discussed.

OCIS codes: (060.6595) Photonic crystal fibers; (060.2370) Fiber optics sensors; (250.5403) Plasmonics;

http://dx.doi.org/10.1364/AOP.0.000000

1. Introduction

Plasmonics, a bridging technology for electronics and photonics, has been extensively studied and widely explored for nanophotonics, magneto-optic data storage, microscopy, solar cells, and sensing applications such as biological and chemical detection [1, 2]. Surface plasmon (SP) waves are coupled electron-photon modes at the boundaries between a metal and a dielectric. Generally, plasmonic sensing devices are categorized into two types: propagating surface plasmon resonance (SPR) sensors and localized surface plasmon resonance (LSPR) sensors. Because of the momentum mismatch between SPs and photons propagating in vacuum, special configurations are needed to excite the plasmon modes.

Compared with prism coupling in traditional bulk-optic systems, the SPR optical fiber offers a more compact and robust configuration with potential in remote and *in situ* monitoring applications. The first SPR optical fiber was proposed and demonstrated in 1993. It showed comparable sensitivity to bulk SPR systems, thus paving a promising path for the development of plasmonic fiber optic technology and applications [3]. Since then, numerous plasmonic fiber optic structures based on simulation and experimental studies have been reported in literature. Various fiber types such as single mode fibers (SMFs) [4], multimode fibers (MMFs) [5, 6], hollow fibers or capillaries [7, 8], tapered fibers [9, 10, 11], U-shaped fibers [12, 13], D-shape fibers [14, 15], side-polished fibers [16, 17] and fiber tips [18, 19] have been demonstrated for enhancing the sensor performance. Fiber grating technologies have also been incorporated to further improve sensitivity, and multiple channel sensing capability has been demonstrated through fiber Bragg grating SPR sensors [20, 21] and fiber long period grating SPR sensors [22, 23].

Photonic crystal fibers (PCFs), also known as microstructured optical fibers, or holey fibers, contain axially aligned air holes which can be arranged periodically or non-periodically in the cladding region centered on a solid or hollow core. These fibers provide unique features and flexibilities not attainable in conventional optical fibers. Since its discovery in 1996, the past two decades have witnessed substantial development of PCF technology for sensing, communication and medical applications [24, 25]. Particularly for sensing applications, PCFs have attracted significant attention in light of the ever increasing demand for high performance sensing devices [26]. The incorporation of plasmonic structures into PCFs seems a natural move of plasmonic fiber optic technology, as PCFs allow unparalleled flexible control of waveguiding properties through engineering the holey structures. As a desirable platform for plasmonic structures, PCFs enable and enhance many application opportunities in terms of performance and versatility.

The potential impact of plasmonic PCFs has resulted in growing effort in developing new device features for all kinds of applications. The most recent review article on this topic focuses on PCF based surface plasmon resonance (SPR) chemical sensors [27]. Other review articles place focuses on optical fiber sensors with SPR or LSPR structures in general [28, 29, 30, 31, 32]. Therefore, there exists a need to have a comprehensive review on using PCFs as a platform for both SPR and LSPR structures for a wider spectrum of applications including temperature sensors and polarization splitters *etc*. In this review, we first summarize the current state-of-the-art achievements in the design, fabrication and application experiments of plasmonic PCFs. We then identify important research directions for the research community. This review begins with an introduction on the operating principles of plasmonic fibers, then followed by an overview on the progress in fabrication techniques and experimental studies. In the second half of this review, we present a summary on various plasmonic PCF structures, which are classified based on their respective applications with benchmarking, and a discussion on their opportunities and challenges.

2. Operating principle of SPR fibers

Surface plasmon waves (SPWs) are electron oscillations guided by an interface between two materials having negative and positive real parts of permittivity. This type of interface is often implemented with a metal-dielectric layer stack. SPWs can be excited by photons when the parallel optical wave vector matches the propagation constant of the corresponding SPW. In an optimized system, an excited SPW can propagate over a long distance with a significant portion of the optical energy being converted to the guided mode. The basis of SPR, which has been extensively used for sensing applications, indeed arises from this wave vector matching requirement as the extent of energy transfer from photons to SPW is very sensitive to a number of parameters such as refractive index of the

medium adjacent to the metal-dielectric interface. A widely adopted practical realization of the SPR sensor is the Kretschmann configuration [33], in which an inverted metal-coated prism exhibits attenuated total internal reflection (ATR) when matching of wave vectors takes place at the metal-glass interface. The metal commonly used is gold because of its chemical stability. Silver provides better performance, but seldom used in practical systems for the same reason. In the case of optical fiber SPR sensors, efficient coupling can be achieved by exposing the core either by side-polishing [34] or selective etching in hydrofluoric acid [35]. Figure 1 shows a typical SPR sensor configuration based on the Kretschmann and fiber configurations.

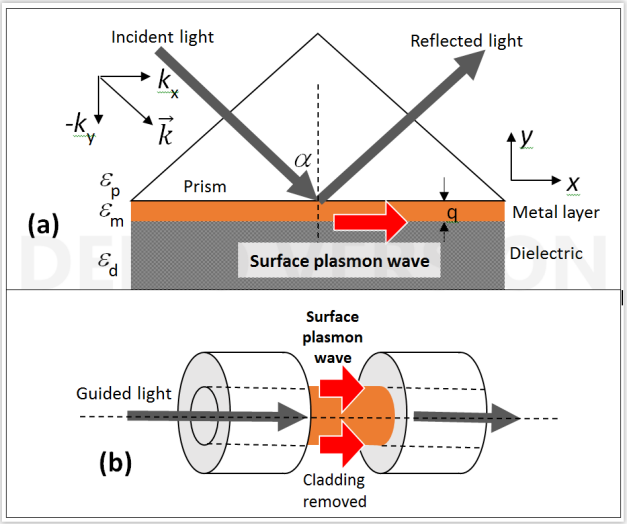

Figure 1. Typical SPR sensor based on the Kretschmann (a) and fiber (b) configurations

Since the excitation of SPWs can be exactly described by the transfer matrix technique, one can readily use the Fresnel's equations [36, 37] to represent the ratio between the incident and reflected electric fields in the system. SPR results in significant optical energy dissipation in the p-polarized component because of coupling of SPW while leaving the s-polarized component unaffected. Equation (1) shows the phase and amplitude of the reflected p-polarized component.

$$r_{pmd} = |r_{pmd}|e^{j\phi} = \frac{E_r}{E_i} = \frac{r_{pm}+r_{md}exp(2iK_{my}q)}{1+r_{pm}r_{md}exp(2iK_{my}q)} \quad (1)$$

where r_{pmd} represents the reflection coefficient of the prism-metal-dielectric structure, $|r_{pmd}|$ the amplitude, ϕ the phase, E_r and E_i respectively the reflected and incident electric filed, q the metal thickness and

$$r_{kl} = \frac{\varepsilon_l k_{ky} - \varepsilon_k k_{ly}}{\varepsilon_l k_{ky} + \varepsilon_k k_{ly}} \quad (2)$$

$$K_{ky} = \sqrt{\left(\frac{2\pi}{\lambda}\right)^2 \varepsilon_k - K_x^2} \quad (3)$$

Here, the subscripts x and y correspond to the coordinate system shown in Figure 1, where k, l are p (prism), m (metal), and d (dielectric), λ is the incident wavelength, K is the propagation constant of the evanescent wave at the prism-metal/metal-dielectric interfaces, and $\varepsilon_p, \varepsilon_m, \varepsilon_d$ the permittivity of the prism, metal and dielectric respectively.

The transfer matrix technique is highly desirable to treat multilayer structures. It is a type of an *ab initio* calculation to get close reproduction of the reflection properties in reality, i.e. a dip in the reflection as described in equation 1 is corresponding to the resonance of surface plasmon excitation.

An intuitive approach is to investigate the dispersion relations of the waves in the waveguides. The propagation constant of the surface plasmon along the metal-dielectric interface is matched to the parallel component of the wave vector in the dielectric. The phase matching conditions in plasmonic fibers are satisfied at the intersections of the effective mode index of the core mode and the surface plasmons. At phase matching wavelengths, the real part of the effective mode index of the fiber waveguide and the surface plasmons are equal. In addition, the confinement loss of the fiber waveguide mode, which is a function of the imaginary part of the effective mode index, would exhibit a peak at the phase matching wavelengths corresponding to surface plasmon excitation.

In metal nanowire filled fiber structures, surface plasmon-polaritons (SPPs) modes can be excited and coupled from the fiber core modes. This structure can be viewed as fiber directional couplers, possessing a dielectric waveguide for core guide mode and a metal wire waveguide for SPP modes. The coupling system generally requires numerical simulation for the electromagnetic wave analysis on dispersion relations and loss properties. The metal wire filled fibers usually possess strong polarization dependent properties. Figure 2 (a) illustrates an example of gold wire filled silica PCF, showing its dispersion relations on the coupling between core mode of the fiber and a few SPP modes of the gold wire in Figure 2(b). At phase matching wavelengths, strong coupling between the core mode and SPP mode can be observed in Figure 2(c), corresponding to peaks (SPP modes excitation) in the confinement loss spectrum as shown in Figure 2(d).

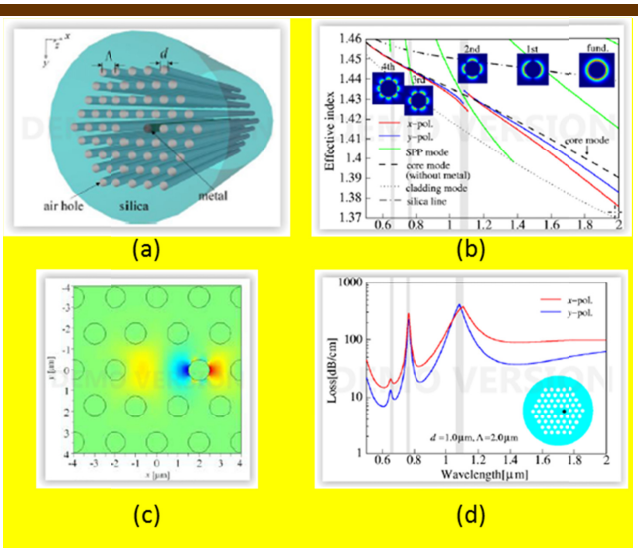

Figure 2 (a) schematic representation of a PCF with a metal wire. (b) Dispersion relations of metal wire filled PCF: *x*-polarized (red curve) and *y*-polarized (blue curve) core modes, the SPP modes of different orders excited on the gold wire (green curves), core mode without metal wire (dash black curve), cladding mode (dotted curve) and index of silica material (dash dotted curve). The SPP mode profiles of the gold wires are shown as inset figures. (c) Mode profile of *x*-component of the electric field distributions of the *x*-polarized core mode at a phase matching wavelength. (d) Confinement loss of the *x*-polarized (red curve) and *y*-polarized (blue curve) core modes. Reprinted with permission from [38]. Copyright 2011 Optical Society of America.

The surface plasmon excitation in thin film coated fibers can be understood from the planar metal-dielectric structure as shown in Figure 1. The guided light in the fiber core would generate evanescent wave at the dielectric-metal interface. The evanescent wave would excite the surface plasmons at resonance wavelengths. An example of metal thin-film coated fiber structure, the dispersion relation and the loss at the proximity of the surface plasmon excitation, and the mode profiles of the fiber waveguide mode and the plasmon mode at the phase matching condition is presented in Figure 3.

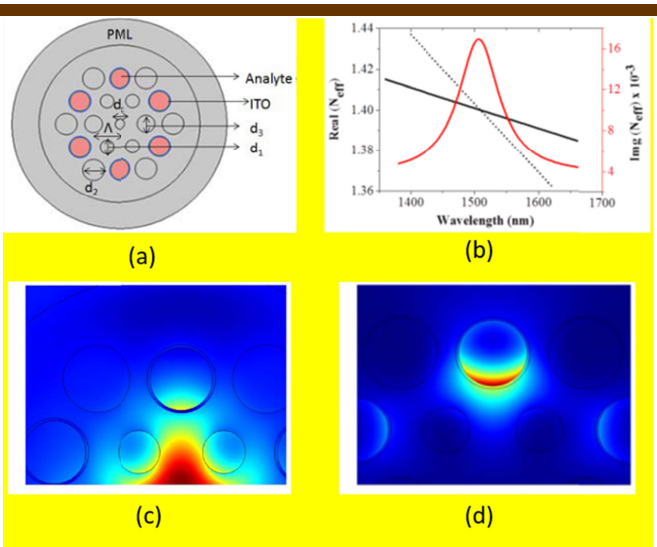

Figure 3 (a) cross section of the proposed sensor. (b) Dispersion relations of core guided mode (black solid line), plasmonic mode (black dotted line) and imaginary part of core guided mode (solid red). (c) plasmonic excitation of core guided mode and (d) plasmon mode. © 2014 IEEE. Reprinted with permission from [39].

Different from propagating surface plasmons, metal nanoparticles (NPs) are embedded for achieving localized SPR (LSPR) within fiber structures. The excitation of LSPR results in highly localized electromagnetic field outside the metal NPs. Numerical simulations are usually required for the analysis of the surface field except for simple systems such as spherical NPs with bigger size, which can be treated by analytical calculations, e.g. Mie theory. Unlike SPR structures, LSPR can be directly excited as the illumination frequency matches the eigenfrequency of the LSPR [40]. A gold nanostar array was designed to achieve wide LSPR band, e.g. 530-620 nm so that could cover both the excitation wavelength and the emission wavelength of Raman scattering [41]. The gold LSPR array design on a fiber facet and the LSPR field intensity and mode profile are presented in Figure 4. The LSPR can be tuned by altering the size, shape and composition of the NPs [41].

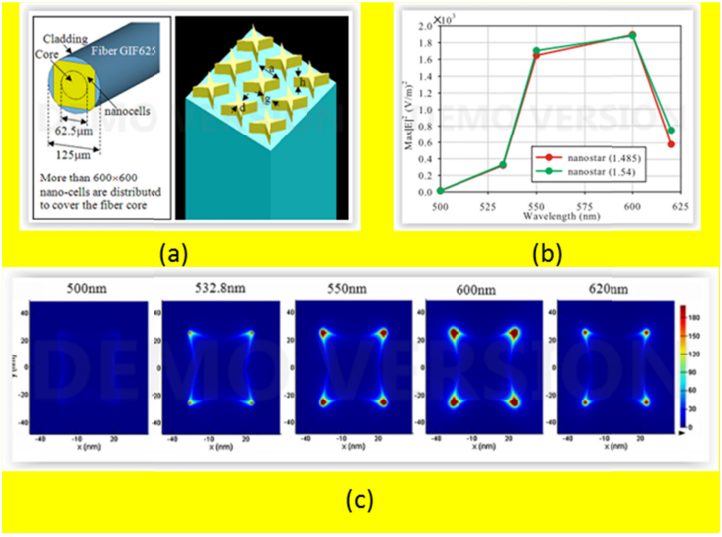

Figure 4 (a) Gold nanostars on a fiber facet with an illustration of 3×3 unit cells. (b) Max|E|² of the 533 nm nanostar at the image plane with incident electric field of 1 V/m. (c) |E|² of the 533 nm nanostar at the image plane with a color bar maximum of 200 (V/m)². Figure reprinted with permission from [41]. Copyright © 2013, Springer-Verlag Berlin Heidelberg. With permission of Springer.

Changes of both the amplitude and the phase under resonance conditions are extremely sensitive to variations in the ambient refractive index n_d (with $n_d = \sqrt{\varepsilon_d}$ if the material is a non-magnetic medium) in the dielectric layer. Due to the dispersive nature of the resonance, spectral response can also be used as a detection parameter. It is the shifts in amplitude, phase and spectral characteristics that constitute the basis of SPR sensors, which is well-known for their high performance in detecting small changes of refractive index on the metal surface caused by conjugation of biomolecular species. This technique has a major advantage over its fluorescence counterparts because of the "label-free" measurement approach. Users may use their samples without having to treat them with fluorescence tags. Moreover, there is no issue associated with photobleaching.

3. Review of fabrication process and experimental studies of plasmonic PCF structures

3.1 Metal nano/microwires filled plasmonic PCF structures

Plasmonic nanowires, such as those made from Au and Ag, are the constituents widely used for creating nanoscale metallic structures in plasmonic waveguides. In a plasmonic fiber structure, guided surface plasmon-polaritons (SPPs) can be excited and supported in metallic nanowires when fiber core guided modes are phase-matched to the SPP modes, thus resulting in distinct resonances of fiber core guided modes. The fabrication of metallic nanowires in a PCF, can be done during [42, 43] or after [44] [45] [46] [47] the PCF drawing process.

The drawing approach was achieved through incorporating the Taylor-wire process [48] into the stack-and-draw procedure for silica PCFs and Polymethyl Methacrylate (PMMA) fibers [42, 43]. Firstly, six silica-coated copper rods were stacked together with 114 hollow capillaries around a single solid silica rod to form the structure of interest. The stack was inserted into another silica tube for high temperature drawing. Scanning electron microscopy (SEM) images of the fabricated PCF with six copper wires are shown in Figure 5. The copper wire diameter was around 4 μm [42]. Tuniz *et al.* demonstrated a co-drawing of PMMA PCFs with polymethyl-methacrylate and indium, and experimentally showed that the polarization dependent transmission property of the fiber was useful for THz filtering and polarizer applications [43]. The fiber drawing method was also shown to be useful for the fabrication of metallic nanowires and microwire arrays [49, 50]. Apart from the Taylor-wire process, a gold filled cane was used to fabricate high-quality gold wires of diameter down to 260 nm and length more than 100 m in standard step index fibers through direct drawing [51]. This method permits more precise control over fabrication parameters, e.g. location of the gold wire in the fiber [51].

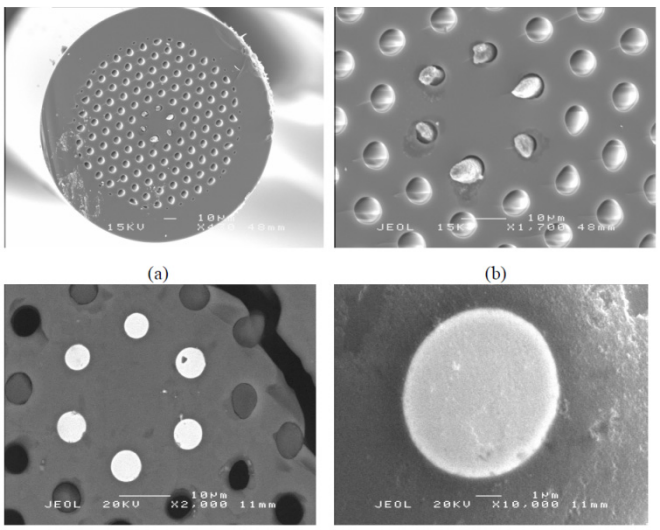

(a) (b) (c) (d)

Figure 5. SEM images of metallic optical fiber with one ring of copper rods. a) shows a cleaved fiber end-face with six copper wires protruding from the surface. b) is a higher magnification image of the six copper wires. c) is a backscattered electron image of the polished fiber sample end-face. d) shows details of the copper rods in c). Reprinted with permission from [42]. Copyright 2008 Optical Society of America.

High-pressure microfluidic chemical deposition technique was employed to fabricate silicon tube and germanium wire filled PCFs [44]. In this approach, high pressure was used to generate mass transport of gas phase precursors through the length of fiber.

Two other fabrication methods for filling the hollow channels with metals and making metallic nanowires within the PCF channel without the need of organic precursors have been reported later. Namely, the techniques are based on high temperature pressure cell [45, 46] and pressure-assisted splicing [47]. The first one was introduced for producing high purity metal nanowire arrays within PCFs though pumping molten metal from a high-temperature (around 1100 ^{o}C) pressure cell into hollow channels of PCFs under high pressure up to 60 bars. The smallest nanowire diameter realized in the experiment was 550 nm. Up to 40 mm penetration lengths of the nanowires were achieved with excellent optical quality. SEM images of the end-face of gold-filled PCF is shown in Figure 6. The PCF structure has been well preserved because the melting temperatures of the metals, e.g. Au and Ag are well below the softening temperature of silica [45].

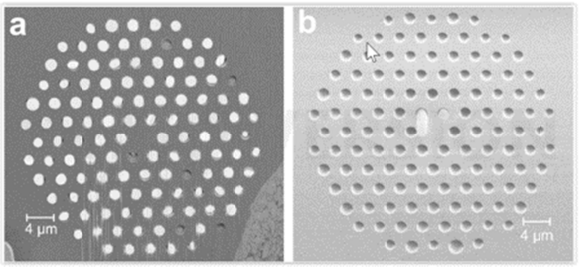

Figure 6. (a) SEM of the end face of a cleaved metal-filled PCF, polished by focused ion beam etching (hole diameter of 1.52 µm, hole spacing of 2.9 µm). The wires undergo ductile thinning during cleaving, breaking at random positions. Those that protrude from the end face are polished and appear as bright disks in the SEM; the rest (six in total) are dull in appearance. (b) SEM image of the unpolished end face of a PCF with two metal nanowires located next to the solid core . Reprinted with permission from [45]. Copyright 2008 by the American Physical Society. https://doi.org/10.1103/PhysRevB.77.033417

The high temperature pressure cell technique was used for selective infiltration of individual air holes with gold nanowires by post processing the PCF structure before pumping in the molten metal. The post-processing technique was based on inflating a PCF heated on a tapering rig, and pressurizing the holes from one end while the other end is sealed [52]. A polarization-maintaining PCF was selectively blocked using the post-processing technique and subsequently infiltrated with gold nanowires using the pressure cell technique at pressures up to 190 bars, with a 900nm diameter gold wire length up to 20 mm. Due to SPR coupling, highly polarization- and wavelength-dependent transmission was observed [46].

The second technique was based on splicing a PCF to a filling capillary having an outer and inner diameter of 200 µm and 80 µm containing a metallic wire, typically at a diameter of 50 µm [47]. The metal wire was manually inserted into the capillary and pushed further into the capillary, leaving an empty section for splicing. The end portion of the capillary was cleaved and spliced to a silica PCF using Vytran splicing machine. Argon gas at a pressure of several hundred bars was applied to push the molten metal into the hollow channels. This method is suitable for non-wetting materials, for example Au, Ag, Ga, Ge and chalcogenide glasses, which have melting temperatures significantly lower than the softening temperature of silica. Selective infiltration of metallic wire can be realized by using an intermediate capillary as a mask between the filling capillary and the PCF. Wires with diameters as small as 120 nm were realized in the experiment. The aforementioned methods were reported to fabricate metal nano/microwires with diameters ranging between 120 nm to 4 µm and length up to 20 cm, as a permanent part of the fiber to form desirable plasmonic PCF structures [47]. This technique has successfully produced a fully filled solid core PCF, a selectively filled PCF, and a modified step index fiber with a parallel gold nanowire were fabricated, as shown in Figure 7 [47]. A transmission measurement setup consisting of a supercontinuum source and an optical spectrum analyser was used to characterize the transmission characteristics of the as-fabricated gold wire-filled PCF. By using a polarizer and a half-wave plate between the light source and the fiber, the input polarization was precisely controlled. The intensity distribution of the SPPs and the polarization characteristics in a PCF with gold nanowire array were measured using a scanning near-field optical microscopy [53]. A single wire-filled and a double wire-filled PCF were measured and showed polarization dependent attenuation spectra. Polarization splitting was observed for the double wire-filled PCF [54].

More recently, Jain *et al.* reported fabrication of micron sized gold nickel alloy wire in a graded index silica fiber by pressure assisted melt filling technique to address the mechanical and chemical weakness of pure metals [55]. The fiber contained a germanium oxide doped graded core and an empty channel parallel to the core, which was filled with the gold nickel alloy using pressure assisted melt filling technique.

Instead of fabricating a metal nanowire structure within PCF, Lu *et al.* reported preparation of silver nanowire solutions in ethanol and chloroform for infiltration in PCF for temperature sensing measurements [56, 57]. In this approach, the authors used capillary effects in the air holes to drive the liquid into the channels, with a penetration depth up to several centimeters. In the experiment, the silver nanowire colloid was a stable translucent colloidal suspension of silver nanowires in ethanol carrier. The liquid was regarded as a physical mixture of ethanol and chloroform. The diameter of the nanowires was about 90 nm, and the average length was about 30 μm. The mixing volume ratio of the silver nanowire solution and the chloroform was changed to tune the plasmonic resonance and the transmission loss.

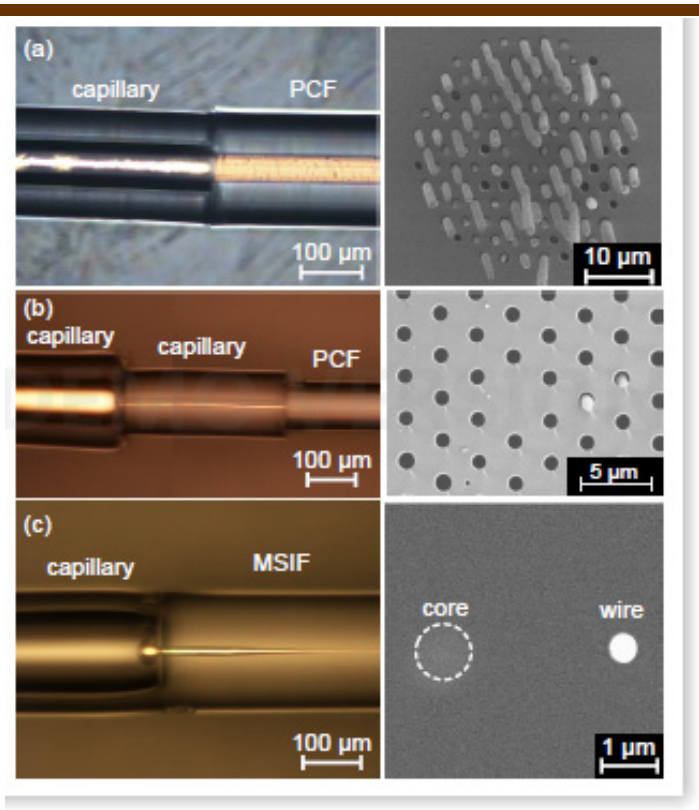

Figure 7. Optical side-views of the splices (left-hand column) and SEM images of the cleaved end-faces (right-hand column). (a) Solid-core PCF with all its channels filled with Au. (b) PCF in which only two channels are filled with Au. (c) Modified step index fiber with a parallel gold nanowire. Reprinted with permission from [47]. Copyright 2011 Optical Society of America.

The characteristics of the metal wires in different PCFs structures are summarized in Table 1. Depending on different fabrication conditions, e.g. temperature, pressure and usage of precursor, metal wire filled PCF have been reported mainly on silica and PMMA PCFs, and various metal materials, showing different outcome of the metal wire characteristics, e.g. diameter and length.

Table 1
Characteristics of the metal wire filled PCFs

Fabrication technique	Wire diameter (μm)	Wire length (mm)	Fabrication condition	Features and properties[1]	Ref.
Modified stack-and-draw technique (combination of Taylor-wire process)	4.2	70	High temperature, e.g. 1880°C	Silica PCF with single or a few copper microwires. The attenuation was measured.	Hou 2008 [42]
Modified stack-and-draw technique (combination of Taylor-wire process)	<10	Up to kilometer	Low temperature, e.g. 156.6°C	PMMA fiber with Indium wire array, Transmittance was measured via THz time domain spectroscopy.	Tuniz 2010 [43]
Pressure assisted melt filling technique	1.3	Up to 8.1	High temperature, e.g. 1100 °C, High pressure, e.g. 50 bar	Silica fiber with AuNi micron sized wire array. The attenuation was measured by cut-back technique.	Jain 2016 [55]
High-pressure microfluidic chemical deposition technique	5	Several cm	High temperature at 700°C, High pressure, organic precursor, e.g. GeH4 germane precursor at 2 MPa partial pressure in Ar was flowing at a total pressure of 40 MPa	Silica PCF with silicone and germanium microwires. The deposited material was studied by Raman spectroscopy; Electrical characterization was conducted on resistivity and carrier type, mobility and concentration.	Finlayson 2007 [44]
High temperature pressure cell technique	0.55	Up to 40	High temperature, e.g. 1100°C, high pressure, e.g. 60 bar	Silica PCF with single and multiple sub-micron Au or Ag wires. The SPR excitation and coupling from fiber core mode was characterized by transmission spectrum measurement.	Schmidt 2008 [45]
	0.9	24.5		Silica PCF with single sub-micron Au wires. Due to SPR coupling, highly polarization- and wavelength-dependent transmission was observed.	Lee 2008 [46]
Pressure-assisted splicing technique	0.12-4	Up to 200	Filling pressure of 300 bar	Silica PCF with multiple sub-micron and micron Au wires. Optical transmission spectra was measured	Lee 2011 [47]

[1] Unless mentioned, the plasmonic effects in the fibers were not studied in the work.

				and showed dips at wavelengths where guided surface plasmon modes on the nanowire phase match to the glass core mode.	
				The intensity distribution of the SPPs and the polarization characteristics in a PCF with gold nanowire array were measured using a scanning near-field optical microscopy.	Uebel 2012 [53]
				A single wire-filled and a double wire-filled PCF were measured and showed polarization dependent attenuation spectra. Polarization splitting was observed for the double wire-filled PCF .	Lee 2012 [54]
Combined method of fiber drawing with advanced filling materials	0.05	1.5 meter	High temperature at 850 ℃	Zinc microwires embedded in glass matrices; the microwires were analysed by taking SEM and energy-dispersive X-ray spectroscopy.	Zhang 2008 [49]
Iterative co-drawing of multimaterial in polymer matrices	0.015	A few hundreds meters	Low temperature <240 °C	Semiconducting and piezoelectric nanowire and nanotube arrays in polymer matrix; the electrical and photoconductivity was measured.	Yaman 2011 [50]
Capillary effect infiltration technique	0.09	0.03	Infiltrated in room temperature	Ag nanowires mixed in solution. The SPR induced resonance was measured for sensing applications.	Lu [56, 57]

3.2 Metal coated plasmonic PCF structures

Successful deposition of metallic layers and/or semiconductors inside PCF structures with high precision is a major step toward the realization of all-fiber optoelectronics. Indeed, the chemical vapor deposition (CVD) approach is a well-established technique for conducting highly controlled deposition of semiconductors and metals from chemical precursors. Sazio *et al.* reported high quality conformal deposition of semiconductor and metal within the voids of PCFs through high-pressure microfluidic chemical deposition [58]. The air holes of PCFs acted as micro/nanoscale CVD reaction chambers. Very high pressure levels ranging from 10 to 100 MPa were used to facilitate rapid mass transport inside the fiber pores. Figure 8 (a) shows the formation of a 80-nm-thick smooth annular gold layer on top of another CVD-deposited silicon tube, thus leading to the formation of a Schottky junction, inside a PCF by means of sequential deposition. One can individually address the holes to produce customized material films on each capillary wall, thus opening the possibility to form patterned plasmonic PCFs. Figure 8 (b) shows an array of gold particles written with a 1.6 μm capillary.

Boehm *et al.* reported an optimized chemical coating method based on the silver mirror reaction (also known as the Tollens reaction) for silver deposition in the internal surfaces of PCFs. The Tollens reaction was optimized to coat 60 nm thick silver layer over a 1-m-length suspended core fiber with three large holes around the solid core [59].

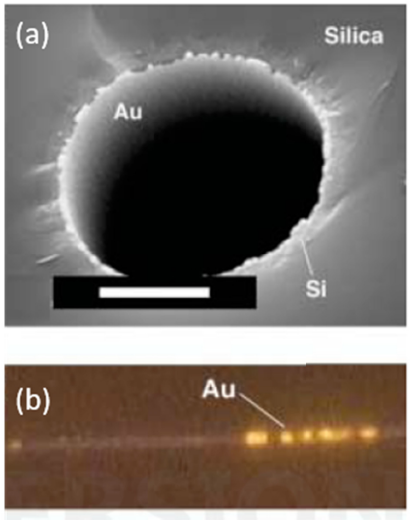

Figure 8 (a) An 80-nm thick smooth gold annulus deposited on a silicon tube. Contrast between silica and silicon is low. Scale bar, 2 mm. (b) Optical micrograph of an array of gold particles written with a focused 514.5-nm laser beam within a 1.6-mm capillary. From [58]. Reprinted with permission from AAAS.

A two-stage draw process was used in the fabrication of microstructured polymer optical fiber (mPOF). A selective silver coating was realized by suction and evaporation of metal nanoparticle mixtures into the desirable holes in the fiber preform with other holes plugged with glue. The reaction mixture was an aqueous solution of dextrose and silver nitrate. Zhang *et al.* used this technique to demonstrate selective silver coating in an mPOF up to 40 cm of penetration into the length of the fiber. However, the coating was rough and granular as shown in Figure 9 [60].

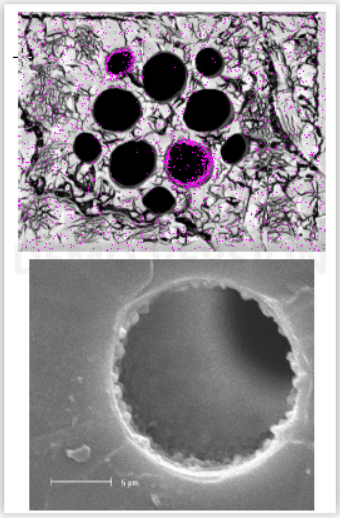

Figure 9 Low magnification SEM micrograph of plasmonic mPOF, showing two coated holes (top). Elemental analysis shows the presence of silver (dots in the image). SEM image of the silver surface of a coated hole is shown on the bottom. Reprinted with permission from [60]. Copyright 2007 Optical Society of America.

Instead of depositing high quality metal films inside the holes of PCFs, some groups proposed to deposit metallic coating outside the fiber. The primary challenge is to produce efficient excitation of surface plasmon from the guided mode, which can be achieved by bringing the metallic coating closer to the fiber modes for efficient coupling. One possible structure is an exposed core holey fiber, which is a modified suspended core fiber where one side of the core is exposed axially. Klantsataya *et al.* reported an experimental demonstration of fabricating thin silver film on the exposed core of the PCF using an electroless plating method involving pre-treatment step and electroless plating process [61]. The fiber samples were thoroughly cleaned and sensitized, and subsequently treated with precipitation of metallic silver from ammoniacal silver nitrate solution in the presence of a reducing agent. An SEM image of the exposed core PCF and the plasmonic PCF structure with silver thin film depositions are shown in Figure 10. Approximately 50 nm-thick silver thin film was deposited on a 1 cm-long mPOF. This deposition technique can be used for multiple sensor fabrication up to 10-15 samples. The plasmonic fiber was enclosed in a flow cell for liquid measurement, showing refractive index sensitivity of 1800 nm/RIU [61]. A similar structure of side hole polymer PCF was reported for SPR sensing, comprising holey cladding, and a side hole to expose the core so that direct sputtering of gold was able to deposit the desired metal layer on the core surface [62].

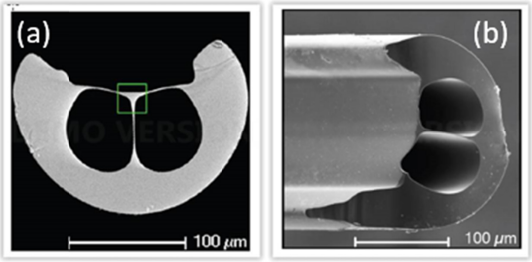

Figure10 (a) Exposed core fiber (ECF) cross section with a triangular core, (b) Silver film deposited on ECF [61]. © 2015 by MDPI (http://www.mdpi.org). Reproduction is permitted for noncommercial purposes

Partial cladding can be etched or side polished from the fiber to enhance evanescent field for surface plasmon excitation. A PCF was side polished by 57 μm and the polished surface was subsequently sputtered with gold to form a thin layer around 34-35 nm in thickness [63]. The fabricated plasmonic

PCF structure was then tested for fluorescence spectroscopy detection of Rhodamine B (RhB) with concentration from 10 μM to 100 μM using the surface plasmon effect.

Partial or complete collapsing of holey cladding enables excitation of higher order modes to reach the outer surface of the PCF. This technique is popular for producing PCF interferometers for liquid detection and biosensing [64, 65]. Wong *et al.* employed this technique in developing a plasmonic PCF biosensor [66]. The PCF sample was spliced between two multimode fibers, with a fully collapsed zone over length of 126 μm. The fiber was then cleaned, dried, and fixed onto a platform for sputtering gold coating around its surface. The gold coated PCF was subsequently chemically treated to form thiol and protein G coating on the gold surface, and used to measure the binding kinetics of the IgG (anti-IgG) complexes with a minimum detection limit at concentration of 0.267 mg/L of anti-IgG.

Tapered PCFs with subwavelength core can provide substantially enhanced evanescent field. A metalized nanostructured PCF taper with gold film perforated on the cross-section of the taper using thermal evaporation technique was reported to show enhanced transmission peaks in the spectral domain [67]. The characteristics of the metal coatings in different PCFs structures are summarized in Table 2.

Table 2
Characteristics of the metal coated PCFs

Fabrication technique	Coating thickness (nm)	Coating length (mm)	Fabrication condition	Features and properties[2]	Ref.
High pressure microfluidic chemical deposition	25	70	High pressure, e.g. 10-100 MPa; organic precursor, e.g. GeH_4, SiH_4; High temperature, e.g. 700°C	Conformal coating of germanium, silicon in silica PCF; Transconductance measurements were carried out to characterize the performance of the semiconductor structure fabricated in the PCF.	Sazio 2006 [58]
Chemical deposition by Tollens reaction	60	1 meter	Room temperature, Medium pressure, e.g. 100 psi	Suspended core fiber with silver coating; The angular position of SPR features were measured for a slide with chemically deposited silver and a slide coated using sputtering, the fiber was not measured for SPR signal.	Boehm 2011 [59]
Two-step fiber drawing method	Granular coating	40 cm	Low temperature, e.g. for polymer fiber drawing	Polymer PCF with selective silver coating. The polarization-dependent transmission of the silver coated fiber was experimentally measured.	Zhang 2007 [60]
Chemical plating technique	50	10	Precipitation of metallic silver form ammoniacal silver nitrate solution	Exposed core silica fiber with silver coating; Performance of the sensor in terms of its refractive index sensitivity and full width at half maximum (FWHM) of SPR response were experimentally investigated.	Klantsataya 2015 [61]
Sputtering technique	37	6	Ar-ion physical sputtering	Polymer side hole PCF with gold	Wang 2009 [62]

[2] Unless mentioned, the plasmonic effects in the fibers were not studied in the work.

				coating; SPR features were experimentally measured for fluid sensing.	
	34-35	10.5		D-shaped silica PCF with gold coating; The SPR field enhancement of the fiber sensor was experimentally demonstrated with an improvement in fluorescence emission intensity and higher sensitivity in fluorescence spectroscopy.	Yu 2011 [63]
	30, 50, 60	5-20		Gold externally coated PCF; The structure was experimentally demonstrated as a SPR biosensor to monitor the binding kinetics of the IgG (anti-IgG) complexes.	Wong 2013 [66]
Thermal evaporation technique	15-200	-	Vacuum	Gold coated on cleaved end of a tapered PCF; A white light was coupled into the PCF side to produce an enhanced optical transmission in the spectral domain through the plasmonic structure at the tapered end.	Arabi 2011 [67]

3.3 Plasmonic PCF structures with nanoparticles

Nanoparticles (NPs) have been extensively studied for applications involving localized surface plasmon resonance (LSPR), in particular surface-enhanced Raman scattering (SERS) due to its unique molecular specificity. The combination of plasmonic nanoparticles and PCFs offers the unique benefit of working with extremely low sample volume and long interaction length. Clearly there exists captivating advantages and promises for developing fully integrated plasmonic devices especially for sensing applications.

The most straightforward method for NP deposition on the inner surface of PCFs is to infiltrate the NP solution into the air holes by capillary effect. After a heating and drying process, the NPs are attached to the inner surface by the opposite charge affinity [68]. The PCF is subsequently filled with the analyte solution. Fiber structures with immobilized NPs are categorized as coated PCFs thereafter. Using this method, Yan *et al*. reported a solid core photonic crystal fiber (SCPCF) with four large air holes surrounding the solid core and surface coated with gold NPs for SERS detection [69]. The NPs can be mixed with the analyte solution and filled into the air channels of PCFs, which does not require a drying process. Structures fabricated with this technique are categorized as liquid filled SCPCFs. Xie *et al*. reported a silver NPs filled SCPCF SERS probe for detection of the 4-Mercaptobenzoic acid solution [70]. Zhang *et al*. demonstrated an ultra-low SERS detection limit of 50 fM using an optimized SCPCF structure filled with gold NPs and Rhodamine 6G (R6G) solution [71].

Hollow core PCFs (HCPCFs) were introduced in the design of SERS detector probes at the same time in order to address a few challenges faced by SCPCFs, which include weak evanescent field in the voids for improved Raman signal excitation and suppression of strong Raman background signal from silica [72, 73, 74]. HCPCFs with NPs immobilized on the inner surface of air holes through the infiltration and drying procedures are categorized as coated HCPCFs. Liquid-filled HCPCFs refer to structures that are completely filled with physical mixture of NPs and analyte. The geometry of silver NPs was optimized for enhanced SERS detection in a liquid filled HCPCF [75]. Improvements of SERS performance were made by sealing/collapsing the air holes in the cladding and infiltrating the hollow core with mixed solution of NPs and analyte for forming a liquid core photonic crystal fiber (LCPCF) [76, 77, 78]. The enhancement was attributed to increased SERS active volume as a result of good confinement of both light and analyte in the central core. Higher sensitivity was later demonstrated using an inner wall-coated LCPCF probe with a sandwich structure, i.e. two types of silver NPs were used as SERS substrates simultaneously. The hollow core was selectively coated with NPs first and selectively filled with a mixed solution of NPs and the analyte [79]. Only the central core was filled/coated with NPs in LCPCFs. A more detailed review of HCPCF-based SERS probes can be found in [80].

The infiltration process can also be assisted with a differential pressure, which was reported by Du's group in the development of a forward-propagating full-length SERS-active SCPCF platform with immobilized and discrete silver NPs [81, 82]. By adjusting the launching condition, an improved SERS signal was demonstrated in a SCPCF coated with gold NPs [83]. Khetani *et al*. reported a differential pressure system for repetitive characterization of a HCPCF Raman probe and experimentally determined HC-PCF filling time is inversely proportional to the pressure difference across the HCPCF in the range of 15 to 60 psi [84].

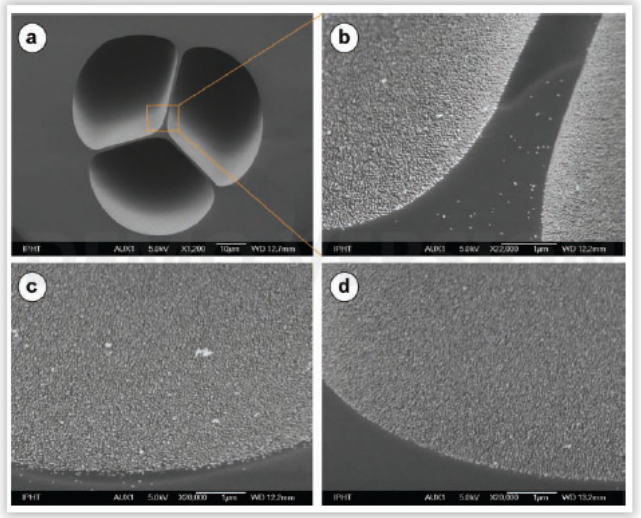

Figure 11. SEM images of the inner walls coated with gold nanoparticles: a) An overview and b) zoomed in. c) Tilted front view of one hole's cross section at the starting point. d) A view of the fiber end [85]. Copyright Wiley-VCH Verlag GmbH & Co. KGaA. Reproduced with permission.

A dynamic low pressure chemical deposition technique for NP layer deposition was reported by Csaki *et al.* and Schröder *et al.*, who used a combination of self-assemble monolayer technique and microfluidics [85] [86]. The inner walls of PCFs were chemically modified by the perfusion of the silanes, acting as a chemical adhesive layer for metal NPs due to its amino modification. The NP solutions were then incubated by continuous flow. The coating uniformity, e.g. the NP density and the layer thickness was constant up to 6 m. Figure 11 shows the homogeneous coating density on the local curvature of the capillary-channel cross section and NP monolayer at saturation coverage [85].

The high pressure chemical deposition technique was reported by Amezcua-Correa *et al.*, employing an organic solvent under high pressure to deliver a silver precursor complex into the fiber holes, followed by a simple thermal reduction of the precursor to form an annular deposition of silver nanoparticles inside the holes. Figure 12 shows the SEM images of silver coating layers achieved by different experimental parameters [87]. The PCFs were typically NP-coated over 15 cm with the central 5–6 cm having the most uniform filling. Their work highlighted the importance of optimized PCF structure with high numerical aperture for efficient collection and detection of Raman response, low loss core guided modes with large optical component propagating in the voids for large excitation area and long interaction length for improved SERS sensitivity. Optimized fiber structures with increased field-particle overlap were investigated for SERS enhancement by Peacock *et al.* [88].

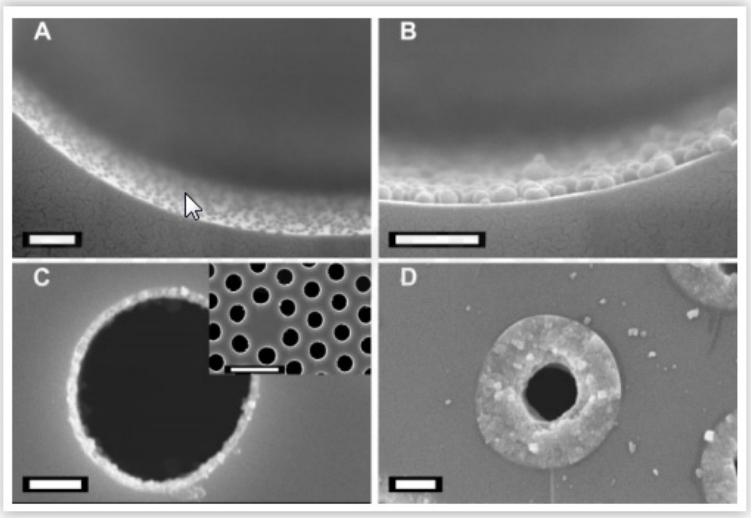

Figure 12. SEM images showing a range of silver deposition profiles obtained by tuning the experimental parameters. A) Deposition Time = 0.5 h with a precursor concentration of 5 mg mL^{-1}; 1 µm scale bar. B) Deposition Time = 0.5 h with a precursor concentration of 10 mg mL^{-1}; scale bar is 1 µm. C) Deposition Time = 2 h with a precursor concentration of 10 mg mL^{-1}; scale bars are 2 µm and 20 µm on the inset. D) Deposition Time = 3 h with a precursor concentration of 15 mg mL^{-1}; 2 µm scale bar. Reproduced with permission from [87]. Copyright © 2007 WILEY-VCH Verlag GmbH & Co. KGaA, Weinheim.

Using the stack-and-draw technique, Bigot *et al.* fabricated a PCF doped with gold NPs by combining a gold NPs-doped silica core rod with capillaries drawing from silica tubes [89]. Sol-gel route was used to synthesize a cylindrical rod with interconnected nanometric pores, which was subsequently doped with gold NPs. The gold NPs-doped core rod was surrounded by silica capillaries to form a preform and drawn into a plasmonic fiber.

The integration of the NP-based SERS substrates in PCF platform has resulted in many successful demonstrations of sensitive, rapid and compact biosensors for bacterial detection, e.g. S. oneidensis [30] and various cancer biomarkers detection including Epidermal growth factor receptors (EGFR) [90], serological liver cancer biomarkers [91], leukaemia cells [92] and sialic acid [93].

The performance figures of the demonstrated NP-based plasmonic PCF devices are summarized in Table 3. The PCFs possess a triangular lattice cladding unless otherwise stated in the table.

Table 3
Performance figures of NP-based plasmonic PCF sensors

PCF characteristics	NPs	Measurand and techniques	Sensitivity	Reference
Coated suspended core fiber (SCF) with three large holes	Au	Refractive index (RI) based on resonance shift	78 nm/RIU	Csaki 2010 [85]
Coated SCF with three large holes	Au[3]	RI based on resonance shift Crystal violet based on SERS	80 nm/RIU 100 μM	Schröder 2012 [86]
Coated hollow core photonic crystal fiber (HCPCF)	Au	Rhodamine B (RhB) based on SERS	10^{-5}M	Yan 2006 [72]
Coated solid core photonic crystal fiber (SCPCF) with four large holes in a triangular lattice cladding	Au	RhB based on SERS	10^{-7}M	Yan 2008 [69]
Coated SCPCF	Au	RhB based on SERS	10^{-7}M	Zhang 2013 [83]
Liquid filled HCPCF with a kagome lattice cladding	Ag	Rhodamine 6G (R6G) based on SERS	$2.1x10^{-7}$M	Cox 2007 [73]
Liquid core photonic crystal fiber (LCPCF)	Ag	R6G based on SERS human insulin based on SERS tryptophan based on SERS	$10^{-4} \sim 10^{-5}$ M	Zhang 2007 [76]
Inner wall coated-LCPCF	Ag	R6G based on SERS	10^{-6} M	Shi 2008 [79]
Coated SCPCF	Ag	R6G based on SERS	$2x10^{-6}$ M	Oo 2009 [82]
Coated SCPCF Coated HCPCF	Ag	R6G based on SERS	10^{-7} M	Han 2010 [74]
Coated SCPCF Coated steering-wheel PCF with three large holes	Ag	R6G based on SERS	10^{-6} M	Oo 2010 [81]

[3] The fibers were coated with different types of NPs, e.g. Au, Ag. The Au NP-coated SCF was tested for sensor measurement.

Coated SCF with three large holes			10^{-6} M 10^{-10} M	
Liquid-filled HCPCF LCPCF	Ag	R6G based on SERS	10^{-7} M 10^{-10} M	Yang 2010 [78]
Liquid-filled HCPCF	Ag	R6G based on SERS	10^{-3}M	Tiwari 2014 [75]
Coated SCF with three large holes	Ag-Au core -shell	R6G based on SERS	10^{-7} M	Pinkhasova 2015 [94]
Liquid filled SCPCF with a side channel in a triangular lattice cladding	Gold	R6G based on SERS	$5x10^{-14}$ M	zhang 2016 [71]
Coated SCPCF	Ag	Benzenethiol based on SERS	1 mM	Amezcua-Correa 2007 [87]
LCPCF	ZnO	polyacrylic acid (PAA) based on Raman spectroscopy	1 mM	Irizar 2008 [77]
Coated SCPCF	Ag	4-aminothiophenol (4-ATP)	0.5 mM	Peacock 2008 [88]
Liquid filled SCPCF	Ag	4-Mercaptobenzoic acid based on SERS	10^{-6} M	Xie 2009 [70]
LCPCF	Ag	S. oneidensis MR-1 strain (bacterial) based on SERS	106 cells/mL	Yang 2011 [30]
Doped SCPCF	Au	Absorption coefficient based on direct measurement of optical attenuation	$0.84x10^{-12}$ cm/W	Bigot 2011 [89]
Protein coated HCPCF[4]	AuNP core SERS nanotag[5]	Epidermal growth factor receptors (EGFRs) based on SERS	10 µg /mL	Dinish 2012 [90]
Protein coated HCPCF	AuNP core SERS nanotag	Serological cancer biomarkers based on SERS	200 µg /mL	Dinish 2014 [91]

[4] The inner wall of the air holes was coated with protein (analyte) first, followed by infiltration of SERS nanotag solutions

[5] The SERS nanotag was constructed by absorbing malachite green isothiocyanate (MGITC) molecule onto the gold NPs followed by bioconjugation.

Liquid filled HCPCF	Ag	Leukemia cells based on SERS	300 cells/ml	Khetani2015 [92]
Liquid filled SCPCF with a side channel in a triangular lattice cladding	Au	Sialic acid based on SERS	2 fM	Gong 2015 [93]

4. Review of plasmonic PCF designs for various applications

Various designs of plasmonic PCF structures have been proposed to achieve desirable characteristics, e.g. sensitivity, detection range, stability, miniaturization *etc.* for a wide range of applications including measurement of refractive index (RI), dual or multi-analyte sensing, temperature sensing, dual parameter sensing, biosensing, polarization devices and couplers. In this section, the plasmonic PCF designs are categorized and reviewed based on their target applications. Gold and silver are two commonly used metals for SPR sensors. Gold or silver coated SPR sensors are investigated in visible wavelengths where the plasma frequencies of both materials are located. Specifically, gold is favoured because of its availability, chemical stability and strong SPR signal which results in good detection sensitivity. On the other hand, silver has a sharp resonance peak which offers better performance in terms of detection sensitivity.

4.1 Refractive index sensing and biosensing

The phase matching condition of the plasmonic and fiber modes is ultrasensitive to refractive index (RI). This property has generated immense interest in the exploration of plasmonic fiber designs for RI sensing applications. High RI sensitivity is a key enabler to develop biosensing devices. In 2014, a review paper overviewed PCF-based SPR chemical sensor designs categorized by three types of metallic structures and various PCF structures [27]. In this section, the pioneering and key designs are emphasized and designs reported from 2014 and onwards are presented. The key designs were selected based on authors' perspectives with the best effort to represent plasmonic PCF designs of the same class.

Phase matching conditions in plasmonic fiber sensors are assessed at the intersections of the effective mode index of the core mode and the surface plasmons, i.e. at phase matching wavelength, the real part of the effective mode index of the fiber waveguide and the surface plasmons are equal. An important parameter, i.e. the confinement loss which is related to the imaginary part of the effective mode index of the fiber waveguide mode, is usually used for characterization of the plasmonic sensor, especially for amplitude interrogation and wavelength interrogation methods.

The confinement loss of the waveguide core modes can be obtained from equation (4):

$$\alpha = 8.686 \times \frac{2\pi}{\lambda} Im\left(n_{eff}\right) \times 10^4 \quad (4)$$

where λ is the operating wavelength in μm, and the unit for α is dB/cm. The confinement loss spectrum of a plasmonic fiber sensor exhibits one or more loss peaks, corresponding to mode couplings to surface plasmons. The loss can be monitored and measured in amplitude change at a particular wavelength. The sensitivity using amplitude based detection method can be defined in equation (5)

$$S_A(\lambda)[RIU^{-1}] = \frac{1}{P(L,\lambda,n_a)} \frac{\partial P(L,\lambda,n_a)}{\partial n_a} = \frac{1}{\alpha(\lambda,n_a)} \frac{\partial \alpha(\lambda,n_a)}{\partial n_a} \quad (5)$$

where α is the confinement loss which is defined in equation 4, and $\partial\alpha$ is the loss variation, ∂n_a is the analyte RI variation. Amplitude interrogation requires simple experimental setup since only intensity measurement is involved. The detection resolution is normally obtained with an assumption of 1% of transmission intensity can be detected reliably and accurately.

In addition to amplitude variation, the loss peak wavelength can also be monitored and measured for varying RI in the wavelength interrogation method. The sensitivity is defined in equation (6)

$$S_\lambda[nm \cdot RIU^{-1}] = \frac{d\lambda_{peak}(n_a)}{dn_a} \quad (6)$$

where $d\lambda_{peak}$ is the shift of the wavelength of the loss peak. The detection resolution is calculated with an assumption of 0.1 nm resonance wavelength peak can be detected reliably with good accuracy. Figure of Merit (FOM) takes the full-width half-maximum (FWHM) of the plasmonic peak into account as well as the absolution resonance wavelength shift, therefore it provides a more comprehensive description of the sensitivity. The definition of FOM is given in equation (7)

$$FOM = \frac{S\ (nm/RIU)}{FWHM\ (nm)} \quad (7)$$

where S is the RI sensitivity obtained by wavelength interrogation, and FWHM is the full width half-maximum of the resonance peak in the loss spectra.

Another important interrogation technique is called phase interrogation which offers higher sensitivity but narrower detection range. The phase shift or phase difference between two polarized waveguide modes per unit sensor length is calculated by equation (8), and the phase sensitivity is calculated using equation (9).

$$\phi_d = \frac{2\pi}{\lambda}\left(Re(n_{TM}) - Re(n_{TE})\right) \quad (8)$$

$$S_\phi[deg \cdot RIU^{-1} \cdot cm^{-1}] = \frac{d\phi_d(n_a)}{dn_a} \quad (9)$$

where Re(n_{TM}) and Re(n_{TE}) are the real part of the effective indices of TM mode and TE mode respectively. The unit for the phase sensitivity is deg/RIU/cm. The peak phase sensitivity occurs in the vicinity of the resonance peak.

The optimization of the sensor performance for a particular PCF structure is carried out by varying a few key parameters, namely metal layer thickness, size and shape of the metal wire, size of the metal nanoparticles, pitch and diameter of the air holes. The finite element method (FEM) is commonly used for simulation studies of the sensor structure due to its capability in modelling complex structures with high spatial resolution.

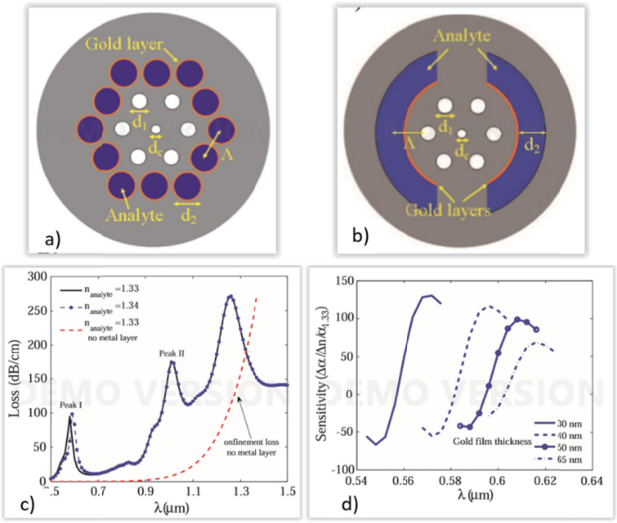

Figure 13. Schematics of PCF-based SPR sensors with a central void in the core region, and a) two layers of air holes in the cladding, the second layer air holes are metal coated and analyte filled. B) one layer of air holes and two large metal coated analyte filled channels. c) Calculated loss spectra of the MOF core guided mode exhibiting three loss peaks corresponding to the excitation of various plasmonic modes in the metallized holes. Black solid line - na = 1.33, blue dotted line - na = 1.34. For comparison, red dashed-line shows the confinement loss of a core guided mode in the absence of a metal coating. d) Sensitivity of the MOF-based SPR sensor for the 30nm, 40nm, 50nm and 65 nm thicknesses of a gold coating. Reprinted with permission from [95]. Copyright 2006 Optical Society of America.

The first proposal of using PCF-based SPR sensor for RI measurement was reported by Hassani *et al.*, laying out the basis of enforcing phase matching conditions between plasmon and fiber core mode using solid core PCF designs [95, 96]. The primary challenge was to enable a highly integrated plasmonic fiber sensor to operate in a desirable wavelength. Generally, the effective RI of a plasmon is close to that of the analyte, e.g. ~1.33 in the case of water, whereas a solid core PCF has an effective mode index close to 1.45. In order to lower the effective index of the fiber core mode, they introduced a void in the core region so that the phase matching of the core mode and the plasmon wave can be obtained. Metallized holes with large size were introduced as the second layer of the holey cladding, forming the optofluidic channels for flowing and detecting the analyte. The schematic of the proposed fiber designs are shown in Figure 13 (a, b). Unlike planar metalized surface which supports only one plasmonic peak, multiple plasmonic peaks in the loss spectra of the fiber core mode correspond to excitation of different plasmonic modes supported by the cylindrical metal layer. The loss spectra of the PCF structure Fi.g 13(a) has three peaks as shown in Figure 13 (c). As the first peak is most sensitive to variation of analyte RI, thus it is usually used as monitoring parameter for detecting RI change of the analyte. In addition, the sensitivity depends weakly on the gold layer thickness as seen in Figure 13(d). Using amplitude based detection methods, the proposed sensor provided RI sensitivity of 10^{-4} corresponding to 1% change in the transmitted intensity.

Based on the pioneering design with a void in the core region [95], Zheng *et al.* investigated the performance of SPR sensors having silver and gold coated nanolayers in the PCF channels through simulation studies. The first peak in the loss spectra of the Ag- and Au-coated PCFs with changing analyte RI, and the respective resonance wavelength shift for RI sensitivity estimation are shown in Figure 14. The Ag-coated PCF sensor has a sharp resonance peak with a higher RI sensitivity compared to Au-

coated PCF sensor, i.e. 1167 nm/RIU and 984 nm/RIU, respectively. Nevertheless, the Au-coated PCF sensor exhibits better linearity in the analyte RI sensing range of 1.30-1.35 [97].

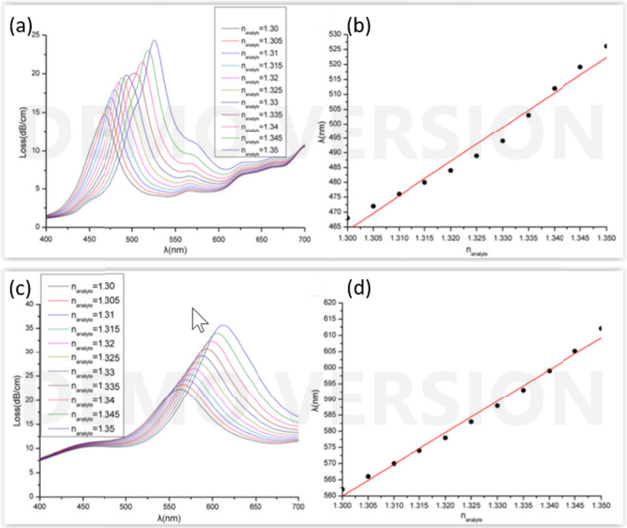

Figure 14. Loss spectra of the fiber core mode as a function of varying analyte RI index, and the relationship between the resonance wavelength and analyte RI in (a, b) Ag-coated PCF, and (c, d) Au-coated PCF. Reprinted from [97], Copyright 2010, with permission from Elsevier .

Optimization of metallic coated air holes in the second layer was proposed to enhance RI detection sensitivity. Yu *et al.* demonstrated enhanced sensor performance in a design in which selectively metallic coated air holes containing analyte channels showed an enhanced RI sensitivity up to 5500 nm/RIU [98]. Wei *et al.* proposed to have six big Ag-coated air holes in the second layer and demonstrated a sensitivity of 1500 nm/RIU in simulation [99]. Another design was proposed by Akowuah *et al.*, utilized a PCF structure consisting a central void in the core region which was surrounded by six air holes including two circular air holes and four elliptical air holes in the cladding, and four metalized microfluidic slots in the second layer. The cross section of the proposed design is shown in Figure 15 (a). The asymmetry of the structure resulted in birefringence in two orthogonal fundamental modes HE_{11}^{x} and HE_{11}^{y}, with spectrally separated phase matching wavelength at 625 nm and 615 nm respectively as shown in Figure 15 (b) of the dispersion relation of the core guided modes and surface plasmons. Figure 15(c-d) shows the plasmonic loss peak shift when the analyte RI varied from 1.33 to 1.34. Based on simulation results, the proposed design provided different RI sensitivity for two polarizations [100]. More recently, Azzam *et al.* investigated the fundamental modes and higher order modes in the PCF structure which were phase matched to plasmons in a similar gold coated PCF structure. Four modes, i.e. HE_{11}^{x}, HE_{11}^{y}, HE_{12}^{x}, and HE_{12}^{y} were analyzed to show an RI sensitivity of 2200, 2400, 2200 and 2400 nm/RIU respectively, thus confirming the proposed design's potential for multi-analyte detection [101].

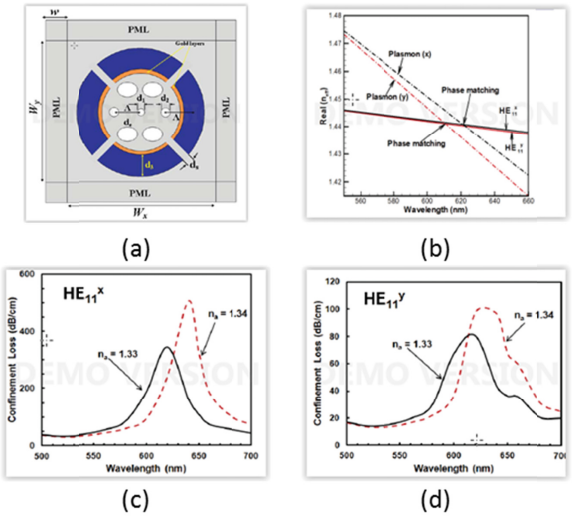

Figure 15. (a) cross section of the proposed PCF design. (b) dispersion relations of core-guided modes and surface plasmon in the vicinity of phase matching point of the first plasmonic peak. (c) Caculated loss spectra of the fundamental mode HE_{11}^{x} and (d) HE_{11}^{y}.

Metallic film deposition on the outer side of the holey PCF was also considered for aqueous detection. Lu *et al.* reported a design based on outer silver coated SPR PCF sensor with RI detection resolution of $8.3 \times 10^{-5} - 9.4 \times 10^{-5}$ RIU [102]. Otupiri *et al.* optimized a PCF structure with a void in the core region, several air holes and two gold coated fluidic slots in the cladding for both the amplitude and wavelength interrogations. Both polarized core modes were considered for phase matching to plasmonic modes because of the symmetry of the gold coated layers. The sensor resolutions were $5 \times 10^{-5} - 6 \times 10^{-5}$ RIU based on wavelength interrogation and $3 \times 10^{-5} - 4 \times 10^{-5}$ RIU based on amplitude interrogation [103]. Rifat *et al.* proposed a birefringent PCF design based on outer gold coated SPR PCF sensor with a void in the center and demonstrated a maximum sensitivity of 4000 nm/RIU and 320 RIU^{-1} respectively [104]. Further improvements of RI sensitivity in such birefringent PCFs were made by optimizing the elliptical ratio of selective air holes in the cladding. Because the built-in high birefringence in the fiber, two polarized fundamental core modes were highly sensitive to the surrounding analyte index, showing RI sensitivity of 6700 nm/RIU and 1000 nm/RIU for the quasi-transverse magnetic and quasi-transverse elelctric modes respectively [105]. A gold coated D-shaped PCF with a void in the core region was optimized with the diameter of the central void as the primary variable in the analysis. It was found that increasing diameter of the central hole can improve the sensitivity in wavelength and amplitude interrogation, but result in reduced phase sensitivity [106].

Near infrared (NIR) wavelengths are favoured for biosensing applications because of their deep penetration depth as well as commercial availability as sources and detectors. Recently, a polymer PCF coated with indium tin oxide (ITO) was proposed to acquire SPR sensing capability at telecommunication window. The polymer substrate was Polymethyl Methacrylate (PMMA). Alternate air holes in the second layer were coated by ITO and filled by analyte and the others were air holes as shown in Figure 2(a). An optimized structure achieved phase matching at around 1510 nm, where mode coupling between the core and SPR modes occurred. The peak of the confinement loss coincided with the phase matching wavelength. The phase matching curve and the electric field profiles of the core and SPR modes are shown in Figure 2(b-d) respectively. The variation of analyte RI affected the phase matching wavelength and confinement loss, which provided the basis for RI detection of the analyte. The results showed that RI sensitivity based on the proposed sensor was up to 2000 nm/RIU [39].

Designs based on solid core PCF without central void were explored for RI sensing applications. Much effort was dedicated to improve RI detection range. Zhou *et al.* demonstrated a broadened analyte RI detection range of 1.25 - 1.45 with high sensitivity. The polymer PCF structure has two analyte channels arranged orthogonally in the second layer with only one channel functionalized with gold coating. Mode coupling between the solid core mode and the SPR mode in the gold coated analyte filled channel occurred for RI values lower than that of the core index; while the core mode couples with the resonant mode of the adjacent analyte-filled channel for RI values higher than the core index [107]. Further

broadening of detection range from 1.30 to 1.79 was reported by An *et al.* The glass material was N-LASF9. The holey cladding contained two gold wires filled holes and four large analyte channels [108]. Gao *et al.* presented a SPR PCF design with Ge-doped silica core surrounded by six air holes coated with TiO_2 and gold layers. The TiO_2 film was used to enhance evanescent fields and enable spectral tuning. The RI sensitivity was $2.7 \times 10^{-5} - 5 \times 10^{-5}$ RIU [109]. The SPR resonance characteristics can be controlled by bending. Napiorkowski *et al.* demonstrated higher degree of bend-induced tunability in plasmonic PCFs as compared to conventional optical fibers by leaking the fundamental core mode to metal layer [110].

In addition to the aforementioned designs, other reported solid core PCF structures for enhanced sensor performance include three-hole PCFs or suspended core holey fibers, grapefruit fibers filled with silver nanowires, exposed core grapefruit fibers with bimetallic structure, active PCFs, D-shaped PCFs, highly birefringent PCFs and U-shaped PCFs.

The three-hole PCF or suspended core holey fibers were proposed for SPR sensing for liquid analyte. An auxiliary low index dielectric layer was sandwiched between the inner wall of the PCF and the gold film deposition to optimize the overlap between the fundamental core mode and the gold layer. The proposed structure was able to achieve the refractive-index resolution 1×10^{-4} for aqueous analytes [111]. Grapefruit fibers filled with silver nanowires were optimized to achieve RI sensitivity of 2400 nm/RIU [112]. Silver nanowires with radius of 300 nm were considered in the proposed design, and one or multiple silver nanowires were used in each grapefruit hole to generate SPR. Simulation results revealed that sensitivity was better for devices with more than one nanowire in each hole, and was stable for devices with further increase in number of nanowires. A modified grapefruit fiber structure with exposed core was designed for SPR detection of liquid. The commercial grapefruit fiber cross section and the schematic of the exposed core grapefruit fiber are shown in Figure 16. The core access can be obtained by polishing the grapefruit fiber and subsequently deposited with a thin layer of silver film. The sensor was showed to have an extremely high wavelength sensitivity of 13,500 nm/RIU for aqueous analyte over the RI range from 1.33 to 1.42 [113]. Another exposed-core PCF design was modified from the three-hole PCF [111], and a silver wire was placed in the exposed region close to the exposed core. The mode coupling between core mode and surface plasmon from the silver wire was utilized for the RI sensing purpose, showing 2700 nm/RIU and 3000 nm/RIU using wavelength interrogation, 247 RIU^{-1} and 231 RIU^{-1} for amplitude interrogation over RI range of 1.33 to 1.34 for both polarizations [114].

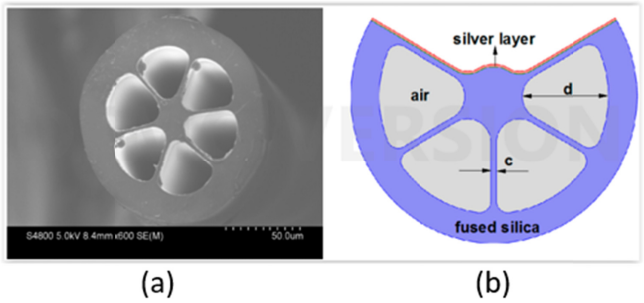

Figure 16. (a) Cross-section of the commercial grapefruit fiber; (b) Schematic of the designed EC-GF-based SPR sensor [113].

An active Yb^{3+} doped solid core PCF with four large analyte channels filled with silver nanowires surrounding the core and air hole arrays in the cladding was proposed in a linear laser cavity. The sensing system was based on the measurement of the laser output power which was influenced by the analyte RI [115].

Solid core PCFs with a D-shaped cladding can be produced by chemical etching method or side polishing method. They allow external deposition of metallic film on a flat and smooth surface, which is easier to achieve and control compared to metallic depositions in the internal walls in PCFs in fabrications, especially compared to designs with selective metallic coating and analyte infiltration in the air holes. The aqueous analyte can be measured external to the metal coated polished surface. Unlike the PCFs with a holey cladding in triangular lattice, An *et al.* proposed a D-shaped PCF with air holes arrayed in rectangular lattice in the cladding layer, and a thin layer of gold film coated on the side polished surface. The proposed sensor was able to provide RI sensitivity up to 8129 nm/RIU and 2000 nm/RIU

in RI range from 1.35 to 1.41 and range from 1.31 to 1.35 respectively [116]. Wang *et al*. optimized the gold coated D-shaped PCF and demonstrated enhanced sensor performance up to 12459 nm/RIU for analyte RI from 1.345 to 1.410 [117].

As an effort to achieve sharp resonance peaks and narrow spectral width, Peng *et al*. optimized a D-shaped PCF sensor with rectangular lattice and two large air holes in the first layer of holey cladding. High sensitivity up to 7481 nm/RIU and narrow full-width at half-maximum (FWHM) 13.6 nm were achieved [118]. Tan *et al.* adopted an experimental setup of phase interrogation in the sensor design, and investigated the phase shift in an all-solid D-shaped SPR PCF. The low-index rods reduced the effective index of the cladding thus enabled a modified total internal reflection in the fiber structure. The sensor achieved a sensitivity of 9.09×10^4 degree/RIU and an improved detection limit of 2.2×10^{-6} RIU at analyte index 1.353 [119]. A comparison between phase interrogation and wavelength interrogation for an elliptical core D-shaped PCF-based plasmonic sensor was presented by Shi *et al.* It was found that the wavelength interrogation could offer a wider dynamic range and higher upper detection limit but much lower sensitivity than those obtained in phase interrogation [120].

Dash *et al*. reported an ITO-coated D-shaped SPR PCF sensor for detection in NIR region where the plasma frequency of ITO lies. The resonance wavelength of the mode coupling between the core mode and the SPR mode shifted from 1688 to 1982 nm as analyte RI varied from 1.33 to 1.37, providing RI sensitivity of 5200 nm/RIU [121]. Further improvement was demonstrated using an ITO-coated birefringent D-shaped PCF. Both wavelength interrogation and amplitude interrogation were analyzed for the structure, showing detection resolution of 17000 nm/RIU and 74 RIU^{-1}, respectively [122]. Recently, Huang optimized the ITO-coated birefringent D-shaped PCF, and demonstrated RI sensitivities of 6000 nm/RIU, 148 RIU^{-1}, and 1.2×10^6 degree/RIU/cm for RI range from 1.30 to 1.31 by wavelength interrogation, amplitude interrogation and phase interrogation respectively [123].

Considering the wide adoption of highly birefringent PCF for SPR fiber sensors, Zhang *et al.* presented a detailed analysis on the suppression of polarization cross-talk by large birefringence. The plasmonic PCF structure under investigation and the electric field profile of core modes of both polarizations are shown in Figure 17 (a-c). The diameters of the air holes in the cladding and two enlarged air holes in the first layer are d_1 and d_2 respectively. The loss spectra of the plasmonic PCF with two birefringent parameters, d_1/d_2 = 0.95 and 0.4 with analyte RI at 1.38 are plotted in Figure 17(c, d) to show the polarization crosstalk. Specifically, attenuation in polarized core modes and total loss were calculated. Resonance wavelength offset between polarized core modes, together with power losses, induce polarization crosstalk, which will in turn lead to measurement errors. The analysis suggested that a birefringence larger than 2×10^{-4} can reduce the resonant wavelength offset to below 0.5 nm. This greatly enhances the resistance of wavelength interrogation to polarization crosstalk [124]. Birefringence analysis was also proposed for locating the resonance peak, e.g. zero-birefringence [125], or abrupt birefringence turning point [126], thus alleviating the need to analyze the confinement loss spectra.

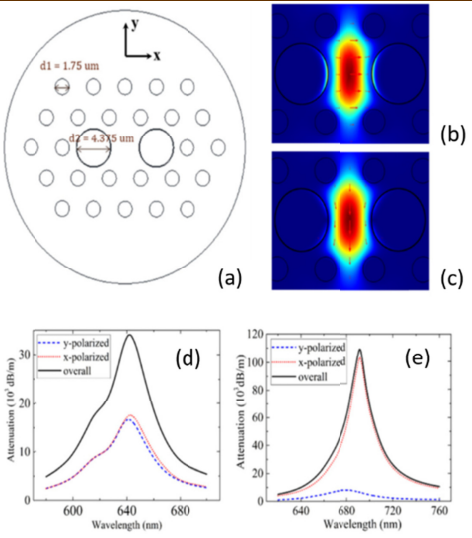

Figure 17 (a) Schematic structure of near-panda PCF based SPR sensor; (b) x-polarized and (c) y-polarized core mode pattern of the proposed SPR sensor; (d-e) Loss spectra of PCF based SPR sensors

when (d) d1/d2= 0.95 (e) d1/d2 = 0.4 with analyte RI at 1.38. Figure reprinted with permission from [124]. https://doi.org/10.1088/2040-8978/18/6/065005

Sensors based U-shaped PCF with a rectangular lattice and gold coating on the U-type trench have been reported. The aqueous analyte detection took place in the trench where SPR wave interacted with the analyte. Both phase interrogation and wavelength interrogation were considered for the proposed design, showing upper detection limit at 1.384 for phase interrogation and figure of merit up to 533.8 RIU^{-1} for wavelength interrogation respectively [127].

Graphene coating has been used to prevent metallic oxidation and also to enhance the sensing performance in plasmonic sensor construction. For examples, silver coated or copper coated PCF sensors with a graphene layer deposition on the metal coating have been reported for enhanced sensor performance. Dash *et al*. reported a PCF structure with a void in the core region, and graphene on silver deposition on the outer layer of the fiber. Other air holes in the fiber were controlled to achieve good confinement and birefringent properties. The analyte detection occurred in the external region to the fiber structure. The sensor performance was shown to be better with higher sensitivity than bimetallic configuration (gold on silver) [128]. The same group reported an improved design by using a D-shaped PCF with similar structure. RI sensitivities of 216 RIU^{-1} and 3700 nm/RIU were obtained by amplitude and wavelength interrogation, which were subsequently proposed for detection of biolayer thickness [129]. Another design was reported by Rifat *et al*, using a PCF with triangular lattice holey cladding, and three high RI analyte-filled cores in a straight line with the central core with graphene on silver coating. Both amplitude and wavelength interrogation methods were considered, and their respective sensitivity levels were 418 RIU^{-1} and 3000 nm/RIU [130]. Yang *et al.* investigated sensor performance of a design based on an analyte-filled and graphene-Ag bi-metal coated PCF with a central air hole in the core region and optimized air holes in the cladding. RI sensitivities of 2520 nm/RIU was demonstrated over RI range of 1.33 to 1.34 [131]. Recently, graphene on copper deposition outside the fiber structure was considered for a plasmonic fiber sensor design. The reported PCF structure has a central void, surrounded by three layers of air holes, which can be readily produced through standard stack-and-draw technique. The graphene-on-copper coating outside the fiber can be obtained by sputtering, CVD deposition method. The proposed sensor was analyzed for both amplitude and wavelength interrogation, and the respective RI sensitivities were 140 RIU^{-1} and 2000 nm/RIU [132].

The void in the core region can be filled with analyte, forming a liquid core PCF as a plasmonic sensing platform especially useful for measuring analyte with RI higher than that of the host material. Zhang *et al*. compared the sensor performance of an analyte filled core PCF with an air filled core PCF, and demonstrated better linearization of the sensor response in a dynamic RI range of 1.33-1.42 [133]. A multicore holey fiber design was proposed by Shuai *et al*., with the gold coated liquid core and holey cladding. Six silica cores were formed by missing of air holes in the triangular lattice. The sensor exhibited better linearity and higher sensitivity in RI range 1.43-1.53 compared to range 1.33-1.42, i.e. 9231 nm/RIU and 2929 nm/RIU respectively [134]. Silver coated multicore holey fiber was subsequently considered and investigated by Liu *et al*., showing an average RI sensitivity of 4500 nm/RIU and 1013 RIU^{-1} for RI range 1.33-1.42 using wavelength and amplitude interrogation, respectively [135].

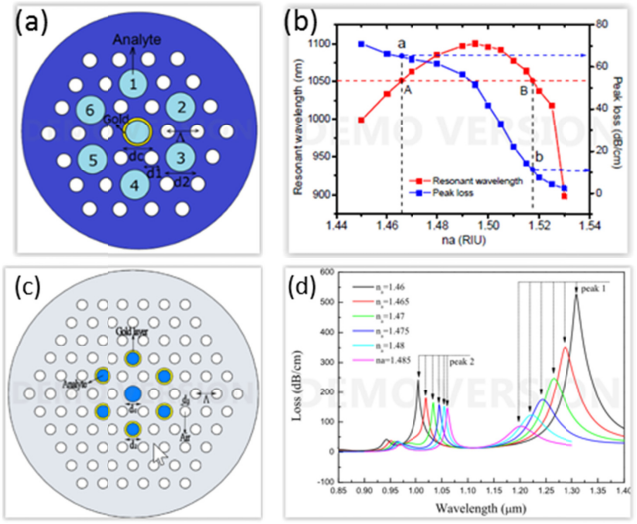

Figure 18 (a) Schematic of a gold coated analyte filled core PCF, (b) RI sensitivity by monitoring the resonance wavelength and peak loss. Reprinted with permission from [136]. Copyright 2012 Optical Society of America. (c) Cross section of the PCF SPR sensor. (d) Loss spectra of the fundamental mode for analyte RI varying from 1.46 to 1.485. Reprinted from [137], Copyright 2014, with permission from Elsevier.

Shuai *et al.* subsequently demonstrated that the analyte RI strongly influenced on the dispersion of both the analyte-filled core mode and the plasmonic mode resulting in the coexistence of positive and negative RI sensitivity in a multi-liquid core PCF based plasmonic sensor. A cross section of the design is shown in Figure 18 (a). The fiber consists of a gold coated core filled with analyte, and three layers of air holes in the cladding. Six holes in the second layer are also filled with analyte to form six liquid cores surrounding the metallized liquid core. This proposed sensor exhibited different properties from the other solid core PCF based plasmonic sensors, in which the resonance peak shifted to longer wavelengths for higher RI analyte with increasing RI sensitivities. Meanwhile, the resonance wavelength experienced a red-shift for RI increasing from 1.45 to 1.495 and a blue-shift for RI increasing from 1.495 to 1.53. By monitoring the peak loss of the core mode in combination with the wavelength interrogation as shown in Figure 18 (b), the analyte RI can be determined [136]. Instead of the triangular lattice, Gandhi *et al.* designed a quasicrystal fiber with an aperiodic arrangement of air holes in the cladding, a gold coated liquid core, and multiple liquid cores in the third layer of the cladding. Coexistence of positive and negative RI sensitivity was also observed in this sensor. The maximum sensitivity was 6000 nm/RIU for low RI range 1.45-1.46, and -4000 nm/RIU for high RI range 1.52-1.53 [138]. Qin *et al.* designed a 'conjugated' PCF SPR sensor with six metalized liquid cores in the second layer of the cladding, and a liquid core in the center as shown in Figure 18 (c). The loss spectra of the liquid core fundamental mode against varying analyte RI is plotted in Figure 18 (d). Two peaks were measured and showing opposite wavelength shifts and reduced peak loss as RI changed from 1.46 to 1.485. Good linearity of the sensor response was obtained. The RI sensitivities of both peaks were -4354.3 nm/RIU and 2280 nm/RIU, respectively. The sensor performance with further increase of the analyte RI was also simulated and showed different RI sensitivities for RI range 1.485-1.50, and 1.50-1.52. Simulation results suggested that the resonance wavelength can be fine-tuned to desirable values by adjusting the structural parameters [137]. Fan *et al.* reported further improvements compared the sensor performance of gold-coated and silver coated PCF sensor. The PCF sensor has an analyte core surrounded by three layers of air holes in the cladding and two metalized core in the second layer. For RI range 1.40-1.42, the gold-coated sensor design showed slightly higher RI sensitivity, i.e. -7040 nm/RIU and -7017 nm. Nevertheless, the silver-coated sensor exhibited sharper loss peak and better figure of merit, i.e. 73.8 RIU^{-1} and 5.9 RIU^{-1} at 1.40 RIU [139]. Tan *et al.* used a different approach compared to previous reports, by filling liquid with controllable RI into the hollow core of a D-shaped PCF which allowed deposition of gold film and subsequent analyte detection external to the fiber structure. The proposed sensor offered an effective way of tailoring the core mode while maintaining the simplicity and robustness of analyte detection. The best sensitivity was found to be 3350 nm/RIU for analyte RI range 1.33-1.34 with the filling liquid with RI of1.39. Further improvement in sensitivity was possible with a filling a high-dispersion liquid [140].

Photonic bandgap PCF-based SPR sensors were studied and optimized for sensing aqueous solutions in visible and near-IR [141, 142]. Several bandgap fiber structures were discussed and analyzed for SPR RI sensing, including solid core Bragg fiber-based SPR sensors with large or small core size, analyte-filled hollow-core Bragg fiber-based SPR sensors, and honeycomb PCF-based SPR sensors. The schematics of the fiber structures are shown in Figure 19. The bandgap guidance enables flexibility in designing any desirable operating wavelength from visible to near IR. Based on simulation results, sensor resolutions in the range $7 \cdot 10^{-6}$-$5 \cdot 10^{-5}$ RIU were demonstrated for an aqueous analyte.

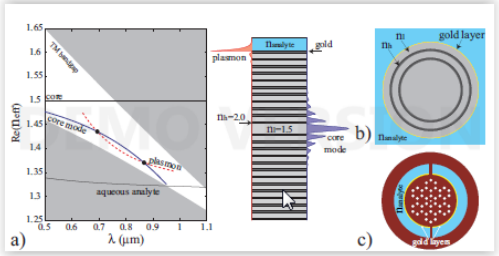

Figure 19 Schematics of photonic crystal waveguide-based SPR sensor schemes. a) Single mode planar photonic crystal waveguide-based SPR sensor. The dispersion relation of the core guided mode is in solid blue, that of the plasmon is in thick dashed red. Inset - coupler schematic; |Sz| of a plasmon (left) and a core mode (right). b) Solid core Bragg fiber-based SPR sensor. c) Microstructured core, honeycomb photonic crystal fiber-based SPR sensor. Reprinted with permission from [141]. Copyright 2007 Optical Society of America.

Tian *et al.* reported a detailed analysis of an all-solid D-shaped PCF structure by looking at the effect of several parameters, including the silver coating thickness, first layer rods and polishing depth on the sensor performance. It should be noted that the guiding mechanism in this design was also based on photonic bandgap effect [143].

Performance comparison between reported designs of plasmonic PCF schemes based on their structures for aqueous analyte RI detection is summarized in Table 4. Due to high loss of the plasmonic fibers based on metal coatings, e.g. ranging from below 100 to 8000 dB/cm, photon propagation is limited to a few hundred microns. Therefore, this kind of sensors should only be considered and developed as an integrated photonic element rather than a fiber [95]. Some designs have relatively lower loss, e.g. below 20 dB/cm, with light propagation of a few millimetres in the structure for sensing purpose and allowing practical fiber handling, such as cleaving and splicing [140] [141]. The design of an exposed core PCF embedded with a single metal nanowire has been shown to offer similar sensitivities compared to metal-coated PCF sensors but with much reduced losses, e.g. 1-5 dB/cm for both polarizations [114]. Therefore, the schemes based on nanowire embedded PCF and metal coated PCF, which have lower loss values, should be explored further for sensing applications in light of their high chance for practical realization.

Table 4

Simulated performance of metal coated plasmonic PCF sensors based on SPR for aqueous analyte RI detection

PCF characteristics	RI range	Interrogation	Sensitivity[6]	Loss[7] (dB/cm)	Resolution (RIU)[8]	Figure of merit (RIU^{-1})	Ref.
Solid core PCF with a void in the core region							
Au-coated	1.33-1.34	Amplitude	100	~180	10^{-4}	-	Hassani 2006 [95]
Au-coated Ag-coated	1.30-1.35	Wavelength	1167 984	~30 ~40	8.57×10^{-5} 1.02×10^{-4}	-	Zheng 2011 [97]
Au-coated	1.33-1.34	Amplitude Wavelength	HE_{11}^{x}: 220 HE_{11}^{y}: 125 HE_{11}^{x}: 2000 HE_{11}^{y}: 1500	~400 ~80	4.54×10^{-5} 8×10^{-5} 5×10^{-5} 6.67×10^{-5}	-	Akowuah 2012 [100]
Au-coated	1.33-.134	Wavelength	HE_{11}^{x}: 2200 HE_{11}^{y}: 2400 HE_{12}^{x}: 2200 HE_{12}^{y}: 2400	>1000	4.54×10^{-5} 4.17×10^{-5} 4.54×10^{-5} 4.17×10^{-5}	-	Azzam 2016 [101]
Au-coated	1.37-1.41	Wavelength	5500	~ 100	10^{-5}	73	Yu 2009 [98]
Ag-coated	1.325-1.345	Wavelength	1500	~140	6.67×10^{-5}	-	Wei 2012 [99]
Ag-coated	1.33-1.335	Wavelength	1064 - 1205	~120	$8.3 \times 10^{-5} - 9.4 \times 10^{-5}$	-	Lu 2013 [102]
Au-coated	1.33-1.34	Wavelength	1667 - 3333	~700	$3 \times 10^{-5} - 6 \times 10^{-5}$	-	Otupiri 2014 [103]
Au-coated	1.33-1.37	Amplitude Wavelength	320 4000	~50	3.13×10^{-5} 2.5×10^{-5}	-	Rifat 2015 [104]

[6] The unit of sensitivity is RIU^{-1}, nm/RIU, deg/RIU/cm for amplitude, wavelength and phase interrogation respectively. Unless otherwise specified, the sensitivity is calculated for the HE_{11}^{y} mode.

[7] It is highly dependent on the order of the plasmonic peak, the metal layer thickness, the fiber geometry and the RI of the analyte. The loss at the first peak of SPR resonance for lowest RI value in the detection range is included in the table. In addition, the value of the loss is indicative only as it varies with different metal layer thickness.

[8] The resolution is calculated by assuming that 1% of change in the transmitted intensity, or a 0.1 *nm* change in resonance wavelength can be accurately and reliably detected in amplitude, wavelength respectively.

Au-coated	1.33-1.34	Amplitude Wavelength	HE_{11}^{x}: 519.4 HE_{11}^{y}: 631.5 HE_{11}^{x}: 10^4 HE_{11}^{y}:6700	~100 ~50	1.925×10^{-5} 1.583×10^{-5} 1×10^{-5} 1.49×10^{-5}	-	Hameed 2016 [105]
Au-coated	1.34-1.48	Wavelength	1131	~100	8.84×10^{-5}	-	Liu 2016 [126]
D-shaped and Au-coated[9]	1.33-1.34	Amplitude Wavelength Phase	120 2900 5.03×10^4	~2000	8.3×10^{-5} 3.4×10^{-5} -	-	Luan 2015 [106]
ITO-coated	1.33-1.35	Amplitude Wavelength	80 2000	~1750	12×10^{-5} 5×10^{-5}	-	Dash 2014 [39]
Solid core PCF without a central void							
Au-coated	1.25-1.383 1.383-1.45	Wavelength	1.4×10^4 2.7×10^4	>360	7.1×10^{-6} 3.7×10^{-6}	-	Zhou 2012 [107]
Au wire	1.30-1.63 1.63-1.79	Wavelength	100 3233	~2500	1.0×10^{-4} 3.09×10^{-5}	-	An 2016 [108]
TiO_2 and Au-coated	1.33-1.35	Amplitude Wavelength	370 2000	~60	2.7×10^{-5} 5×10^{-5}	-	Gao 2014 [109]
Three-hole PCFs Au-coated	1.33-1.34	Amplitude Wavelength	80 1000	~70	1.25×10^{-4} 1×10^{-4}	--	Hautakorpi 2008 [111]
Grapefruit fibers Ag nanowire	1.33-1.335	Wavelength	2400	~700	4.17×10^{-5}	-	Lu 2012 [112]
Exposed core grapefruit fibers Ag-coated	1.33-1.42	Amplitude Wavelength	HE_{11}^{x}: 204 HE_{11}^{y}: 191 HE_{11}^{x}: up to 13500 (not linear) HE_{11}^{y}: up to 12000 (not linear)	~8000 ~1000	4.9×10^{-5} 5.23×10^{-5} 7.4×10^{-6} 8.3×10^{-6}	-	Yang 2015 [113]
Exposed core three hole	1.33-1.34	Amplitude	HE_{11}^{x}: 247	5	4.05×10^{-5}	-	Luan 2016 [114]

[9] The diameter of the central hole is fixed at 0.2Λ in the structure for three interrogation method.

fiber Ag wire[10]		Wavelength	HE_{11}^{y}: 231 HE_{11}^{x}: 2700 HE_{11}^{y}: 3000	1	4.33×10^{-5} 3.70×10^{-5} 3.33×10^{-5}		
D-shaped solid core PCF without a central void							
Au-coated	1.33-1.35 1.35-1.41	Wavelength	2000 8129	~100 ~300	5×10^{-5} 1.23×10^{-5}	-	An 2014 [116]
Au-coated	1.37-1.398	Wavelength	7481	~400	1.34×10^{-5}	478.3	Peng 2015 [118]
Au-coated	1.333-1.357	Phase	6.5×10^{4}	~100	2.2×10^{-6}	-	Tan 2014[11] [119]
Au-coated	1.36-1.41 1.371-1.373	Wavelength Phase	6000 2.2×10^{5}	~1000	1.67×10^{-5} -	-	Shi 2015 [120]
ITO-coated	1.33-1.37	Wavelength	5200	~140	1.92×10^{-5}	-	Dash 2016 [121]
ITO-coated	1.33-1.35	Amplitude Wavelength	74 1.7×10^{4}	~40	1.35×10^{-4} 5.8×10^{-6}	-	Dash 2016 [122]
ITO-coated	1.30-1.31 1.28-1.34 1.28-1.34	Amplitude Wavelength Phase	148 6000 1.2×10^{6}	~1000	6.76×10^{-5} 1.67×10^{-5} -	-	Huang 2016 [123]
Highly birefringent PCFs							
Au-coated	1.33-1.38	Wavelength	3000	~90	3.33×10^{-5}	-	Zhang 2016 [124]
U-shaped PCFs	1.365-1.395 1.382-1.384	Wavelength Phase	$\sim 7.6 \times 10^{3}$ 8.1×10^{4}	~150	1.32×10^{-5} -	533.8	Ge 2016 [127]
Graphene coated PCFs							
Graphene on silver	1.33-1.37	Amplitude	860	~1500	1.16×10^{-5}	-	Dash 2014 [128]
Graphene on silver	1.33-1.37	Amplitude Wavelength	216 3700	~200	4.6×10^{-5} 2.7×10^{-5}	-	Dash 2015 [129]
Graphene on silver	1.46-1.49	Amplitude Wavelength	418 3000	~100	2.39×10^{-5} 3.33×10^{-5}	-	Rifat 2015 [130]
Graphene on silver	1.33-1.34	Wavelength	2520	~100	3.97×10^{-5}	-	Yang 2016 [131]
Graphene on copper	1.33-1.37	Amplitude	140	~50	7.14×10^{-5}	-	Rifat 2016 [132]

[10] This work about a nanowire embedded PCF is included in the table to show the difference in loss as compared to metal coated PCF sensors.

[11] The sensor length was 1.4 cm to provide a 130 dB loss in the sensing region; a noise level of 0.2 degree was assumed for the sensor.

		Wavelength	2000		5×10^{-5}		
Liquid core PCFs							
Au-coated	1.33-1.42	Wavelength	4200 2600	~550	2.38×10^{-5} 3.85×10^{-5}	-	Zhang 2011 [133]
Au-coated	1.33-1.42 1.43-1.53	Wavelength	2929 9231	~32	3.41×10^{-5} 1.08×10^{-5}	-	Shuai 2012 [134]
Ag-coated	1.33-1.42	Amplitude Wavelength	1013 4500	~25	9.87×10^{-5} 2.22×10^{-5}	-	Liu 2015 [135]
Au-coated	1.45-1.46 1.52-1.53	Wavelength	3700 -5500	~70	2.7×10^{-5} 1.82×10^{-5}	- 98.2	Shuai 2012 [136]
Au-coated	1.45-1.49 1.5-1.53	Wavelength	6000 -4000	~0.04	1.67×10^{-5} 2.5×10^{-5}	-	Gandhi 2016 [138]
Au-coated	1.46-1.485 1.485-1.50 1.50-1.52	Wavelength	-4354.3 -3800 -4240	~500	2.3×10^{-5} 2.63×10^{-5} 2.36×10^{-5}	79.2 - -	Qin 2014 [137]
Ag-coated Au-coated	1.40-1.42	Wavelength	-7017 -7040	~700 ~200	1.43×10^{-5} 1.42×10^{-5}	73.8 5.9	Fan 2015 [139]
Au-coated	1.38-1.46	Wavelength	3350	~7	2.99×10^{-5}	-	Tan 2014 [140]
Bandgap PCFs							
Au-coated Large solid core Bragg fiber	1.33-1.34	Amplitude Wavelength	214 1900	~8	4.7×10^{-5} 5.3×10^{-5}	-	Gauvreau 2007 [141]
Au-coated Small solid core Bragg fiber		Amplitude Wavelength	293 1020	~5	3.4×10^{-5} 9.8×10^{-6}	-	
Au-coated Analyte filled Bragg fiber		Amplitude Wavelength	365 7000	~80	2.7×10^{-5} 1.4×10^{-5}	-	
Au-coated honeycomb PCF		Amplitude Wavelength	400 13750	~250	2.5×10^{-5} 7.2×10^{-6}	-	
Ag-coated All solid bandgap fiber	1.33-1.38	wavelength	7300	~60	1.37×10^{-5}	216	Tian 2012 [143]

4.2 Dual or multi-analyte sensing

Multichannel analyte detection by SPR sensors has witnessed development similar to that of SPR sensors for single analyte detection, from bulk prism-coupled configurations to miniaturized fiber optic structures (references on multi-analyte by previous effort). The presence and flexible design of air hole channels enable feasible developments for dual or multi-analyte sensing in PCF-based plasmonic devices, which are favoured by many applications such as clinical diagnostics, drug discovery and environmental monitoring.

The first PCF-based multichannel plasmonic sensor was proposed by Zhang *et al.* in 2011. Similar to an earlier proposed three-hole PCF structure [111], the proposed design introduced modifications of multilayers, e.g. cladding layers with lower refractive index than silica were introduced and subsequently gold layers were deposited uniformly. An overlay layer was introduced on gold coating in channels for sensing purpose. Dual analyte detection was proposed by incorporating two types of sensing layers in the channels, so that channels with different sensing layers exhibited a spectrally differentiable plasmonic loss peak. The numerical results showed average RI sensitivity of 1535 nm/RIU over a RI range of 1.33 to 1.36 for all channels [144].

Another multichannel plasmonic PCF design was proposed by Otupiri *et al.*, with a central void in the core region, surrounded by four rotated elliptical air holes in the first layer and four large gold-coated analyte filled channels in the second cladding layer. Two channels in the horizontal axis were also coated by Ta_2O_5 overlayer underneath the gold coating layer. The Ta_2O_5 and gold coated channel pair were denoted as channel 1 and the gold coated channel pair were denoted as channel 2, which were filled by different analytes. Two plasmonic loss peaks were found and attributed to phase matching between core guide modes and plasmons at channel 1 and 2 for both polarizations. The phase matched wavelengths for *x*-polarized fundamental mode were 675 nm and 900 nm, and 645 nm and 836 nm for *y*-polarized fundamental mode. It was found that *x*-polarized mode had a dominant plasmonic loss peak due to channel 1, whereas the *y*-polarized mode had a dominating peak due to channel 2. By detecting the wavelength shifts of the two plasmonic peaks, dual analyte RI in either channel can be measured. Wavelength interrogation method was used for dual analyte detection mode, showing sensor sensitivities up to 4600 nm/RIU and 2300 nm/RIU for *x*-polarized and *y*-polarized modes. In addition, the sensor can be operated in a self-referencing mode, i.e. in one channel the analyte was fixed, and changes in analyte RI can be measured in the other channel. The amplitude interrogation method was used for the self-referencing mode with RI sensitivities of 425 RIU^{-1} and 131 RIU^{-1} for *x*-polarized and *y*-polarized modes [145].

4.3 Temperature sensing and dual parameter sensing

The high RI sensitivity of plasmonic PCF sensors has motivated researchers in designing and developing plasmonic PCF sensors for sensitive temperature measurement. In 2007, Florous *et al.* proposed to incorporate gold nanoparticles (NPs) in a PCF for temperature sensing. The PCF had a solid core surrounded by two layers of air holes. The localized surface plasmons (LSPs) excited by the propagating core mode, can be temperature tuned as the Au NPs were heated or cooled to result in a wavelength shift in plasmonic peak. The numerical simulations demonstrated the temperature sensitivities of spherical and ellipsoidal Au NP-deposited PCF sensor, showing 0.062 nm/^{o}C and 0.046 nm/^{o}C respectively [146]. The gold nanoparticle deposition could be achieved by techniques discussed in section 3.3.

To enhance the temperature sensitivity, a liquid with high thermos-optic coefficient can be used to completely or selectively fill air holes in the PCFs to induce temperature dependence of the plasmonic response. Depending on the interrogation method of the sensors, the temperature sensitivity can be evaluated by measuring the amplitude, wavelength or phase of the plasmonic resonance.

Silver nanowires filled PCFs were proposed for temperature sensing [147, 148, 57]. The air holes were filled with a mixture of ethanol and chloroform, with a high thermos-optic coefficient of -6.328 x 10^{-4} and -4 x 10^{-4} respectively. By controlling the mixing volume ratio for the infiltration into the air holes of the PCF structure, the desirable temperature sensing range can be tuned. Luan *et al.* proposed a grapefruit PCF filled with Ag nanowires based temperature sensor. The calculated temperature sensitivity was around 4 nm/^{o}C [147]. The influence of the shapes of Ag nanowires was studied by Wang *et al.*, using an octagon PCF structure. Three shapes were considered in the simulation, i.e. circle, ellipse and square, showing temperature sensitivities of 0.25, 0.4 and 0.2 nm/^{o}C from -40-0 ^{o}C, respectively [148]. Yang *et al.* reported both theoretical and experimental investigation of Ag nanowires filled large mode area (LMA) PCF based SPR sensor for temperature sensing. Using a commercially available LMA-10 PCF structure as the sensor platform, the mixing volume ratio of ethanol and chloroform was varied from 1:1 to 1:3, resulting redshift of peak wavelength as well as increase in peak loss for temperature

range 25-60 ^{o}C. The experimental results confirmed the high temperature sensitivity up to -2.0833 nm/^{o}C with an FOM of 0.1572 $^{o}C^{-1}$ [57].

In 2012, Peng *et al.* reported a temperature sensor based on a selective coated SPR PCF. The PCF design contained a void in the central core region, surrounding by two layers of air holes. The second layer of air holes with larger diameters were filled with the sensing medium with large thermos-optic coefficient, i.e. -4 x 10^{-4}, and selectively coated by gold. Numerical calculations suggested a spectral sensitivity of 0.72 nm/^{o}C of the proposed sensor for 0-50 ^{o}C detection range. The gold film thickness played an important role in influencing the FWHM of the loss resonance peaks, while the sensitivity remained stable. Consequently, the FOM obtained by thinner gold film was higher. An optimal coating thickness of 35 nm was suggested by considering the sensor length, loss dynamic range and the FOM [149]. A multi-core PCF with gold-coated liquid filled core was proposed for temperature sensing, achieving good linearity of 0.99991, high sensitivity of -2.15 nm/^{o}C and average FOM of -0.044 $^{o}C^{-1}$ in range of 20-80 ^{o}C [150]. More recently, Hameed *et al.* explored the combination of nematic liquid crystals (NLC) which is highly temperature dependent and PCFs filled with nanowires for temperature sensing. Compared with NLC-filled PCF devices without plasmonic couplings [151, 152], the proposed NLC core SPR PCF design offered a higher temperature sensitivity as well as broader sensing range with linear response [153].

Dual parameter sensing is an important and desirable capability especially for the purpose of differentiating the parameters or minimizing cross talks, e.g. RI and temperature. Most plasmonic PCF sensors for liquid analyte measurement with high RI sensitivity are prone to temperature induced cross talks. To address this challenge, Luan *et al*. used an exposed core PCF with silver layers coated on the exposed core and one air hole next to the core for dual parameters sensing. In the proposed design, a liquid mixture of ethanol and chloroform was filled in the silver coated air hole which was responsible for the temperature sensing; RI of the liquid analyte was measured external to the silver coated exposed core. Two resonance peaks were present for both orthogonal polarizations, with a major peak at 838 nm for x-polarized mode supported by the temperature sensing channel, and a major peak at 535 nm for y-polarized mode supported by the RI sensing channel. Each peak was shifted by temperature or variation e of thanalyte RI respectively. The proposed sensor exhibited RI sensitivity of 1900 nm/RIU for RI range 1.33 to 1.34, and temperature sensitivity of 6.18 nm/^{o}C for temperature range 26-43 ^{o}C [154]. A summary of the plasmonic PCF sensors for temperature measurement is shown in Table 5.

Table 5
The performance of the plasmonic PCF temperature sensors

PCF characteristics	Thermo-optic coefficient ($^oC^{-1}$)	Temperature range (^oC)	Sensitivity (nm/^oC)	FOM ($^oC^{-1}$)	Reference
Solid core PCF with Au NPs deposition on the inner wall of the air holes	-	-173.15-226.85	0.062 (Spherical) 0.046 (Ellipsoidal)	-	Florous 2007 [146]
Selectively Au-coated PCF with a central void	-4×10^{-4}	0-50	0.72	0.013-0.026	Peng 2012 [149]
Multi-core PCF with an Au-coated liquid core	-4.65×10^{-4}	20-80	-2.15	-0.044	Liu 2015 [150]
Grapefruit PCF with six holes filled with Ag nanowires	Ethanol -6.328×10^{-4} Chloroform -4×10^{-4}	-4-15	4	-	Luan 2014 [147]
Octagon PCF filled with Ag nanowires	Ethanol -6.328×10^{-4} Chloroform -4×10^{-4}	-40-0	0.25 (Circle) 0.5 (Ellipse) 0.4 (Square)	-	Wang 2015 [148]
LMA PCF filled with Ag nanowires	Ethanol -6.328×10^{-4} Chloroform -4×10^{-4}	25-60	-2.08	0.135-0.1572	Yang 2016 [57]
Liquid crystal core PCF with Au nanowire	Temperature dependent Cauchy coefficient for NLC E7 [155]	30-50	10	-	Hameed 2016 [153]
Ag-coated exposed core PCF with one Ag coated and liquid filled channel	Ethanol -6.328×10^{-4} Chloroform -4×10^{-4}	26-43	6.18	-	Luan 2016 [154]

4.4 Polarization and birefringent devices

Plasmonic PCFs exhibit high losses in the core modes at phase matched wavelengths due to strong power coupling to surface plasmon polaritons (SPP) modes, inviting substantial interest and effort in developing in fiber filter devices at specific communication wavelengths or broadband communication windows. Various designs of plasmonic PCF structures incorporating metal wires, coatings or nanoparticles (NPs) are reviewed based on the type of metal configuration, and PCF characteristics in this section.

4.4.1 Metal wire filled PCFs

Mode coupling between two orthogonal polarization directions in plasmonic PCFs were studied for polarization splitting by Nagasaki *et al.* Their work investigated the polarization-dependent loss characteristics in a gold wire-filled solid core PCFs with triangular lattice of air holes in the cladding. The core mode could only be coupled to second or higher order surface plasmon polaritons (SPPs). It was found that PCFs with a single gold wire showed similar loss peak wavelengths and loss values for both polarizations. On the contrary, PCF structures with several gold wires selectively filled some air holes, were achieving high polarization extinction ratio desirable for polarization filter applications. The arrangement of the gold wires played an important role in the fiber's polarization dependence. In addition, the diameter of gold wires was increased to achieve large polarization extinction ratio over wide range of wavelengths [38]. The birefringence is a key parameter to decrease the coupling length between the two orthogonal polarization states in order to enhance the polarization splitting. A polarization-maintaining (PM) PCF with triangular lattice of air holes in the cladding with one gold wire filled into one air hole was studied by Du *et al.* The study revealed the relative significance of design parameters namely gold wire positions, gold wire dimension, birefringence strength, and pitch of air holes, on the polarization splitting ratio. By optimizing the fiber geometry and the inclusion of two gold wires in the cladding, complete separation of two polarization dependent plasmonic resonances was demonstrated, thereby making it possible to realize polarization splitting filters operating at communication wavelengths. Two designs were proposed for polarization dependent wavelength filters as shown in Figure 20 (a,b) [156]. A D-shaped PM PCF with a gold nanowire, as shown in Figure 20(c), was used as a polarization filter. The device was operating at communication wavelengths, i.e. 1310 nm and 1550 nm, with crosstalk better than 30 dB and bandwidths at 88 and 150 nm, respectively [157]. Yogalakshimi *et al.* reduced the diameter of the air holes in the inner two layers compared to that of the outer two layers, and demonstrated polarization filtering by controlling the number of gold wires and changing the positions of the gold nanowires. In addition, gold coatings were also used to tune to the desirable peak resonance wavelength and control the absorption loss factor [158]. Ag-Au alloys have been proposed for developing plasmonic devices, utilizing the flexibility of controlling the composition to obtain desirable plasmonic resonance wavelength [159]**.** More recently, tunable narrowband polarization filters were designed based on PCFs with a solid core and the first layer air holes was filled by liquid crystal in the cladding, liquid crystal core or liquid core surrounded by triangular lattice of air holes and gold wires in the cladding. The tunability was achieved by temperature tuning [160]**,** applying external electrical field to control the rotation angle of the liquid crystal as shown in Figure 20 (d) [161] or changing the filled liquid [162].

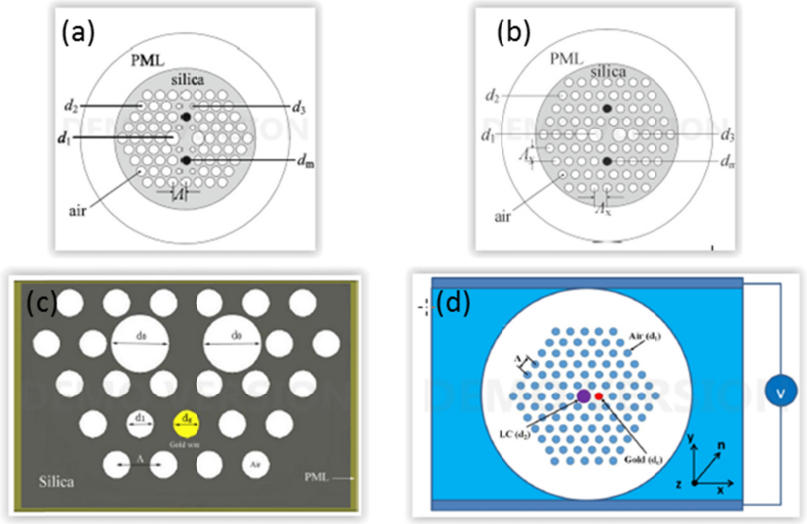

Figure 20. Examples of solid core PCF with triangular lattice and filled with metal wires for polarization filter devices. (a, b) two designs based on birefringent PCFs and two embedded gold wires in the cladding. Figure reprinted with permission from [156], Copyright 2012 With permission of Springer. (c) Schematic diagram of the designed D-PCF with gold nanowire. Figure reprinted with permission from [157],Copyright 2015 With permission of Springer. d) Cross section of the PLC-PCF filter filled with a metal wire and sandwiched between two electrodes. Reprinted with permission from [161]. Copyright 2015 Optical Society of America.

PCFs with air holes in square lattice and filled with metal wires have received significant attention for the development of polarization filtering devices. Zhang *et al.* showed that the size of the gold wire and symmetry of the air holes around the solid core have significant impact on the polarization filtering characteristics. An optimized design with two gold nanowires in the cladding was demonstrated for peak loss up to 279.10 dB/cm and 399.18 dB/cm at wavelengths of 1.02 μm and 1.55 μm [163]. By adjusting the gold wire diameter, An *et al.* proposed a PCF design with solid core surrounded by air holes in square lattice and two gold wires for polarization filter at communication wavelengths 1310 and 1500 nm [164]. Jiang *et al.* designed an ultrashort PCF single polarization wavelength filter of 0.3 mm for communication wavelengths 1310 and 1500 nm. The PCF was filled with a single gold wire next to the solid core in the holey cladding in square lattice. A cross section of the fiber design and the dispersion as well as the modal loss is presented in Figure 21. Fiber core modes were coupled to 2nd-order SPP modes in orthogonal polarizations, resulting in completely separated polarization loss peaks at two wavelengths [165]. A ultra-broadband single polarization filter was reported by the same group using a PCF with a liquid crystal core and filled with single gold wire in the square lattice holey cladding. Simulations suggested that the design was able to achieve high polarization extinction ratio in 1.25-2.1 μm which is desirable for broadband single polarization filter applications [166]. A spiral PCF with an elliptical core and filled with gold wires were investigated by Heikal *et al.*. The study showed that by changing the structural parameters and the number of gold wires, the coupling between core modes and higher order SPP modes can be controlled, offering opportunities for designing polarization dependent wavelength filters [167]. The performance figures of the polarization dependent wavelength filters based on the proposed plasmonic PCF with triangular, square lattice and spiral air holes in the cladding and filled with metal wires are summarized in Table 6.

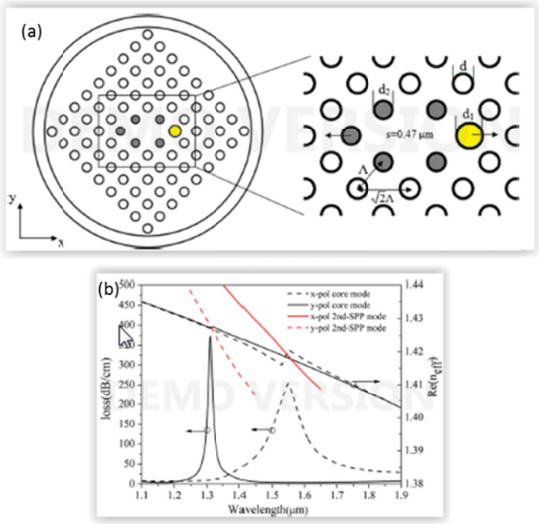

Figure 21. (a) Cross section of the proposed PCF, (b) dispersion and modal loss of the x- and y- polarized core modes. Figure reprinted with permission from [165]. © Springer Science+Business Media New York. Reproduced with permission. All rights reserved.

Table 6

Simulated performance figures of metal wire-based plasmonic PCF polarization splitters

PCF characteristics	Metal wire	*x*-pol: Loss (dB/cm)	*y*-pol: Loss (dB/cm)	Wavelength (nm)	Ref
PM-Solid core PCF with triangular lattice of air holes	Design1. Au	- ~275	~ 400 -	1125 1275	Du 2012 [156]
	Design2. Au	- ~60	~40 -	1295 1550	
D-shaped PCF with PM triangular lattice	Au	4.0 4.6	208.4 249.5	1310 1550	Fan 2014 [157]
Solid core PCF with triangular lattice	Design1. Single Au wire	147.48 302	348.55 140	1520 1560	Yogalakshmi 2016 [158]
	Design2. Two separate Au wires	- 352.84	451.16 -	1520 1560	
	Design3. Two adjacent Au wires	187.67	-	1400	
	Design4. Au coating	<18.52	406.34	1640	
Solid core PCF with triangular lattice	Two Ag/Au alloy wires	24.42	309.14	~1100	Shi 2014 [159]
Solid core PCF with triangular lattice and first layer filled with liquid crystal	Au	0.81	446	1550	Chen 2015 [160]
Liquid crystal core PCF with triangular lattice	Au	600 0.092	0.0075 157.71	1300	Hameed 2015 [161]
Liquid core PCF with triangular lattice	Two Au wires	443.36 309.35 258.34	2.24 6.17 7.86	1310 1490 1550	Liu 2016 [162]

Solid core with square lattice	Two Au wires	279.1 399.18	- -	1020 1550	Zhang 2014 [163]
Solid core with square lattice	Two Au wires	231.6 -	- 237.9	1310 1550	An 2016 [164]
Solid core with square lattice	Single Au wire	9.41 214.31	373.9 3.88	1310 1550	Jiang 2016 [165]
Liquid crystal filled core with square lattice	Single Au wire	>248.95 433.25	<0.21 0.0064	1250-2100 1300	Jiang 2016 [166]
Spiral PCF with elliptic core	Design 1. Single Au wire	80.14 -	- 63.23	950 1183	Heikal 2015 [167]
	Design 2. Multiple Au wire, e.g. 2	94.1 -	- 56.42	980 1400	

Dual core PCFs with gold nanowires are widely explored for achieving polarization filtering characteristics utilizing the difference in resonance coupling characteristics of even and odd supermodes, high birefringence and high polarization dependence in transmission [168] [169] [170] [171] [172] [173] [174] [175] [176]. In a dual core PCF structure, the extinction ratio is defined as the power ratio between the undesired and the desired polarization states in each output port or core.

Zhang *et al.* used supermode theory and the coupled mode theory to confirm the enhancement of the power transfer between two fiber cores due to the presence of a silver wire in between and its associated resonant coupling between surface plasmons and fiber core modes. The coupling characteristics of a gold wire filled and gold coated PCF couplers were investigated, showing coupling ratio up to -30.54 dB between two fiber cores [168]. Li *et al.* investigated the difference in resonance coupling characteristics, dispersion and confinement loss properties for the even and odd supermodes in a dual core PCF with gold wire in between the two cores. Polarization dependent transmission was demonstrated and two orthogonally polarized components can be separated in the proposed gold-filled dual core PCF coupler. Specifically, at 1330 nm, the light is one core was purely *x*-polarized and the other core was purely *y*-polarized after an optimized propagating length, the power ratio of the orthogonal polarizations in each core was around -40 dB [169]. A polarization splitter was demonstrated using a silver wire filled dual core PCF of 63 mm length. The polarization splitting was achieved by designing a dual core plasmonic PCF with coupling length ratio of the two orthogonal polarization states of 2 or ½. The bandwidth of polarization splitting with extinction ratios below -20 dB was over 146 nm wavelength range for both polarizations [170]. Sun *et al.* improved the design to achieve a shorter device length and broader bandwidth of polarization splitting [171]. Khaleue *et al.* investigated highly birefringent PCF structures with two gold wires embedded in the cladding for ultra-broadband polarization splitters [172] [173]. An elliptical metal wire was used in the center of a dual core PCF structure for polarization splitting at 1310 and 1550 nm. The mode couplings occurred for the core guided modes and higher order, i.e. fourth or fifth SPR modes [174]. A broadband polarization splitting device with extinction ratios below -20 dB was over 400 nm wavelength range was demonstrated by Liu *et al.* [175]. A dual core PCF with cladding air holes in square lattice and a gold wire in the center was designed as an ultra-broadband polarization splitter with an extinction ration of -78.2 dB at 1550 nm and bandwidth of 430 nm of ER better than -20 dB [176]. The performance figures of the polarization splitters using dual core PCF structures containing metal wires are summarized in table 7.

Table 7
Performance figures of dual core metal wire-based plasmonic PCFs for polarization splitters

PCF characteristics Metal wire	Length (mm)	ER_x (dB)	ER_y (dB)	Wavelength (nm)	Range (nm) (<-20 dB)	Ref
Dual core triangular lattice PCF						
Ag	-	-30.54	-	1550	-	Zhang 2012 [168]
Au	0.5942	~-40	~-40	1310	-	Li 2013 [169]
Ag	63	-39.4	-35.2	1550	*x*-pol: 1441-1587 *y*-pol: 1430-1605	Sun 2013 [170]
Ag	0.5775	-34	-42	1596	*x*-pol: 1439-1689 *y*-pol: 1421-1700	Sun 2015 [171]
Au	0.2546	-111	-	1550	*x*-pol: 1420-1980	Khaleque 2015 [172]
Au	0.117	-100	-	1550	*x*-pol: 1250-1710	Khaleque 2015 [173]
Au	0.585	-50	-	1320	1270-1670	Liu 2015 [175]
Dual core triangular lattice PCF with elliptical metal wire in the core center						
Au	2.937 0.827	-70 -70	-	1310 1550	*x*-pol: ~1290-1380 ~1475-1575	Fan 2016 [174]

Ag	3.066 0.809	-54 -66	-	1310 1550	*x*-pol: ~1300-1366 ~1480-1570	
Dual core PCF with square lattice						
Au	4.036	-78.2	-	1550	1250-1680	Jiang 2015 [176]

Besides polarization splitting devices, dual core PCF with a gold wire in the fiber center region and infiltration of nematic liquid crystal (NLC) of type E7 in the cladding air holes was designed and demonstrated as a polarization independent wavelength multiplexer and demultiplexer. The two polarized states at 1550 and 1300 nm can be separated [177]. A square lattice PCF with two defects, i.e. a smaller air hole in the first layer and a gold wire in the second layer of the holey cladding was proposed as polarization rotator. The design acted as a dual core plasmonic PCF, containing a silica core and gold wire core which support hybrid supermodes. Simulation results showed that an optimized structure could offer almost 100% polarization conversion ratio at 1550 nm [178].

4.4.2 Metal film coated PCFs and nanoparticles coated PCFs

Compared with metal wire filled PCFs, metal-coated PCFs use less metal and exhibit stronger resonance strength. Therefore, considerable effort has been spent in developing metal coated PCFs for polarization splitter applications for communication wavelengths. For polarization dependent devices, high birefringence in PCFs has been obtained by several techniques, such as introducing the asymmetry of cladding or modified air holes in size or liquid infiltration in the cladding *etc.* Dou *et al.* designed a PCF with rhombic lattice and different lattice pitch along *x*- and *y*- directions for achieving the high birefringence as well as two gold coated air holes in the cladding. By tuning the gold layer thickness, the fiber core mode was coupled to the second order SPP in *y*-polarization state at resonance wavelength 1550 nm with confinement loss of 630.2 dB/cm, whereas that of the x-polarization state was 36.9 dB/cm. A short device length such as 2mm was sufficient to split the polarizations with ER of -118.7 dB [179]. PCF with round lattice was explored for polarization splitter application, showing up to 364.8 dB/cm confinement loss in the *y*-polarization direction at 1550 nm wavelength [180]. Solid core PCFs with triangular lattice and gold coated holes have been proposed for polarization splitting devices, with modifications of one or two gold coated air holes [181] [182] , or liquid filled holes in the cladding [183]. Utilizing the high thermos-optic coefficient of the filled liquid such as glycerin, Wang *et al.* demonstrated a design for both the temperature sensing and polarization splitting [184].

FWHM of the loss curve can be controlled by varying PCF structural parameters or filling liquids, *via* which a broadband polarization filter can be designed [185] [186] [187] [188]. Liu *et al.* realized a broadband polarization filter from 1.25 μm to 2μm with ER smaller than -20 dB with a 1 mm fiber length. The flexibility of controlling the resonance wavelength was also demonstrated by varying gold layer thickness or gold wire diameters in the report [185]. Wang *et al.* designed a broadband polarization filter based on a PCF with a big gold coated hole in the holey cladding. A few other air holes in the cladding were modified in diameter to induce high birefringence and facilitate mode coupling between fiber core mode and SPP mode. The design was shown to exhibit ER lower than -20 dB from 1.26 to 2 μm for device length longer than 0.21 mm [186]**.** Han *et al.* reported a highly birefringent PCF based single polarization singe mode fiber with two gold coated holes filled with liquid in the cladding for broadband polarization splitting [187]. Chen *et al.* reported a D-shaped PM PCF with two big holes next to the solid core and gold coated on the surface for polarization splitter application. A cross section of the proposed fiber is shown in Figure 22 (c). Mode coupling between the fiber core mode and different higher order SPR modes in y-polarized states resulted in different phase matching wavelengths. Particularly for the seventh order SPR mode, the resonance wavelength was 1560 nm. The phase matching plots and corresponding confinement loss of the core mode are shown in Figure 22 (a, b). Considering a 4mm fiber device, an ultra-broadband polarization splitter exceeding 1 μm with ER<-20 dB was achieved as shown in Figure 22 (d) [188].

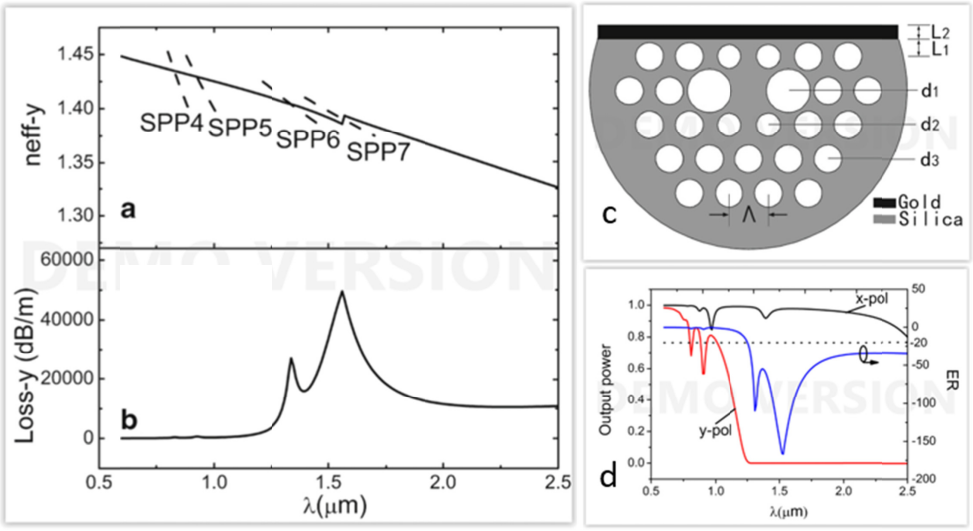

Figure 22 (a) Phase matching between core mode and higher order SPP modes in y-polarization direction. (b) Confinement loss of core mode in y-polarization direction. (c) The schematic of the proposed SPR PCF. (d) The output power and ER of the polarization splitter. The thickness of gold film is 0.05 μm. The transferring length is set as 4 mm. Figure reprinted with permission from [188], Copyright 2015 With permission of Springer.

Chen *et al.* reported an Au film coated D-shaped PCF polarization splitter and the bandwidth were 40 and 60 nm for *x*- and *y*- polarization modes with ER better than -20 dB [189]. Fan *et al.* compared the polarization splitting between a dual core PCF with a gold wire in the center and a dual core PCF with a gold film coated hole in the center, and found that due to stronger resonance coupling in a gold film coated PCF, the bandwidth could reach 220 nm with ER better than -20 dB for a device length of 0.542mm [190].

Square lattice has shown flexibility in controlling the birefringent properties which are desirable for polarization splitters. PCFs one or more gold coated holes in a square lattice cladding have been proposed for polarization splitter at 1310 and 1550 nm [191] [192]. Chen *et al.* investigated a PCF with a solid core by missing three holes in a square lattice structure. The core was surrounded by two gold film coated holes and four large elliptical holes in the first layer. Polarization dependent coupling between the fiber core mode and the SPP mode resulted in desirable polarization splitter performance at communication wavelengths [191]. Another PCF design with one gold film coated hole and a few other holes modified in diameter in the square lattice was shown to improve the polarization splitting at the wavelengths and short device length [192]. There have been reports on PCFs with square lattice rotated by 45 °C [193] [194] [195] [196] and squeezed lattice rotated by 45 °C [197] [198]. Wang *et al.* reported a PCF design with two coated holes in the cladding and demonstrated bandwidth of 800 nm for ER better than -20 dB for a fiber length longer than 0.2 mm [193]. Zi *et al.* designed PCF with squeezed square lattice and two large Au-coated holes on orthogonal corner, and demonstrated bandwidth of 181 nm and 423 nm for wavelength window 1310 nm and 1550 nm, respectively [195]. Liu *et al.* demonstrated an optimized design to achieve high confinement loss of y-polarized core mode at 1310 nm and 1550 nm, up to 452.4 and 102 dB/m, respectively. A 3 mm length device would be able to achieve more than 430 nm bandwidth of ER better than -20 dB [196].

In addition to using metal wires and metal films, metal nanoparticles (NPs) have also been proposed to design for LSPR based polarization filters. Poudereux *et al.* selected a PM-PCF structure filled with a mixture of AgNPs in matrix of Polydimethylsiloxane (PDMS), showing attenuation up to 1200 dB/cm in the *x*-polarization direction and 119 dB/cm in the *y*-polarization direction at the LSPR resonance wavelength around 442 nm. Tuning of the LSPR resonance was also demonstrated through NP size for attenuation amplitude and through temperature for resonance wavelength [199]. Table 8 summarizes the performance of polarization splitters based on Au-coated PCFs. The presented designs usually possess high loss of a few hundred dB/cm for one polarization, while much lower loss for the orthogonal polarization for effective polarization splitting within a very short device length, e.g. sub-millimeter to millimeter scale, which is a challenging task for fabrication. The plasmonic fiber device for polarization filtering and splitting should also be developed as an integrated photonics element rather than a fiber due to their high loss.

Table 8

The performance of gold-coated PCF based polarization splitters

Au-coated PCF characteristics	*x*-pol: [12] Loss (dB/cm)	*y*-pol: Loss (dB/cm)	Wavelength (nm)	Range (nm) (<-20 dB)	Ref.
Solid core with rhombic lattice					
-	630.2	36.9	1550	-	Dou 2015 [179]
PM-solid core PCF with round lattice					
PM	~25	364.8	1550	130 (0.8 mm)	Hao 2016 [180]
Solid core with triangular lattice					
A big gold-coated air hole	-	1362.53 1676.07	1310 1550	-	Wang 2016 [181]
Liquid filled	~20	508.6	1311	-	Xue 2013 [183]
Liquid core, two coated holes in the cladding	2.02 5.29	412.91 536.25	1310 1550	-	Jiang 2015 [182]

[12] Some of the values are not explicitly stated in the paper, we report an estimated value based on the graph presented in the work. The field is left empty if such information is not available from the paper.

One hole filled with glycerin	~100 321.442	445.958 ~100	1400 1480	-	Wang 2016 [184]
Au with different thickness	~20 ~10 ~10	377.19 417.21 418.02	1310 1480 1550	1250-2000 (loss in *y*->350 dB/cm)	Liu 2015 [185]
Modified triangular lattice and a big gold-coated air hole	857.8	-	1310	1260-2000 (>0.21 mm)	Wang 2016 [186]
Two holes filled with liquid	-	~250	~1450	1350-1700 (30 dB/cm)	Han 2015 [187]
D-shaped	~0.5	495.21	1560	1250-2500 (4mm)	Chen 2015 [188]
Dual core PCF with triangular lattice					
D-shaped	-	-	1550	1530-1570 (0.782 mm)	Chen 2015 [189]
Coated hole in the center between dual core	384.6	444.1	1260	1380-1600 (0.542 mm)	Fan 2015 [190]
Solid core with square lattice					
PMPCF with four elliptical holes next to the core and two coated holes in the cladding	102.6 1.7	3.5 245	1310 1550	-	Chen 2014 [191]
One coated hole in the cladding	123.46 -	- 410.04	1310 1550	-	Liu 2015 [192]

Solid core with square lattice rotated by 45 °C					
Two coated holes in the cladding	~20	720	1310	1200-2000 (>0.2mm)	Wang 2015 [193]
Design 1: one large Au-coated hole	-	517 375	1310 1550		Zi 2015 [194]
Design 2: two large Au-coated holes on opposite corner	-	701	1310		
Design 3: two large Au-coated holes on orthogonal corner	~10 369	475 ~20	1310 1550	181 423 (1 mm)	Zi 2015 [195]
Two coated holes in the cladding	- -	452.4 102	1310 1550	430 (3 mm)	Liu 2015 [196]
Squeezed square	1221	1.6	1310	-	Khaleque 2015 [197]
Two Au coated holes, modified squeezed square lattice	771.5	2.7	1310	-	Li 2015 [198]
Metal nanoparticles (NPs)					
PM PCF, the two large holes filled by NPs and PDMS	1200	119	442	-	Poudereux 2015 [199]

4.5 Others

Unlike pure silica glass in which the nonlinear coefficient is a real number and almost constant, composite materials such as gold-silver nanoparticles have complex nonlinear coefficients. The inclusion of composite materials in PCFs leads to unusual nonlinear properties, which is favourable for the study of ultrashort pulse and soliton dynamics [200]. Metal coated silicon nanowire embedded plasmonic PCFs have been shown to support efficient propagation of SPP modes in the nanowire and to have a high threshold power for undesirable free carrier effects, showing potential in Kerr-related nonlinear applications with relative high power [201]. Different from utilizing the plasmonic effects, PCFs with metal nanowire arrays surrounded by a dielectric have been proposed for electromagnetic invisibility. Such metamaterial based fibers possess a refractive index that can be matched to the surroundings [202].

5. Conclusion

Over the past several years, there has been substantial growth in the design, fabrication, and application development of plasmonic PCF devices. The idea is to build a novel class of plasmonic components with enhanced interaction between light and medium, by integrating the capabilities of plasmonics in a robust and flexible PCF platform for sensing and communication applications.

Firstly, substantial development has been made in the fabrication for plasmonic PCFs. Various technologies have been developed for fabrication of metal nanowires filled PCFs, such as modified process of stack-and-draw technique [42], high-pressure microfluidic chemical deposition technique [44], high temperature pressure cell technique [45, 46], pressure-assisted splicing technique [47], and capillary effect of filling nanowires in liquid mixture [56, 57]. The metal coated PCFs have been reported with fabrication techniques including high-pressure microfluidic chemical deposition technique [58], the silver mirror reaction for suspended core PCFs [59], two-stage draw technique for polymer PCFs [60], electroless plating [61], sputtering [62], and thermal evaporation for tapered PCF [67]. NP-coated PCF can be realized by techniques based on capillary effects [68], or assisted by high pressure injection [81, 82], low pressure chemical deposition using a combination of self-assembly and microfluidics [85] [86], high pressure chemical deposition [87] and stack-and-draw [89]. Continuing effort in improving and maturation of fabrication techniques is essential to advance the field and it will drive the realizations and advancements of plasmonic PCF devices and components with better quality, more robustness and higher reliability.

Secondly, diversity of plasmonic PCF designs has flourished in recent years, as can be seen from the wide range of device schemes specifically tailored for many applications including refractive index sensing and biosensing, multi-analyte sensing, temperature sensing, dual parameter sensing and polarization splitter *etc.* Rapid updates have been reported in the benchmarking of device performance, such as sensor sensitivity, polarization splitting extinction ratio and bandwidth *etc*. These efforts have provided a solid foundation for theoretical and experimental investigations, as well as guidance for future device development.

The realizations of the plasmonic PCF structures with intricate designs and features are limited due to the achievable metal structures in fabrication. Firstly, it is difficult to achieve small diameters and high aspect ratio wires in PCFs. Most fabrication methods reported so far produce micron or sub-micron size metal wires up to length scale of cm. Secondly, it remains a challenge for sputtering and evaporation techniques to achieve continuous uniformity of metal coatings inside and outside of the PCFs. Thirdly, better uniformity of metal layer in the PCF was achieved using chemical deposition methods with more complicated conditions, e.g. high pressure, high temperature *etc*. In addition, different fiber materials and structures require different fabrication techniques. For instance, polymer fibers have much lower drawing temperatures compared to silica fibers. PCFs with different fiber structures and metal structures, e.g. air hole size, air filling fraction, single or multiple wires, complete or selective coating, and internal or external fabrication of metal structure in the PCF, all contribute to different requirements or procedures in the fabrication. Lastly, the proposed designs of plasmonic fiber devices, e.g. sensors and polarization splitters are showing extremely high losses associated with very short device lengths of sub-millimeters. However, realization of such plasmonic fiber devices as in-fiber device would require more flexibility in the device length to millimeters or centimeters for practical development. All of the considerations discussed herein should be taken into account in the design process to ensure good feasibility of the plasmonic PCF structure.

It is encouraging to see the vast possibilities in different designs of metallic PCF structures with desirable characteristics in numerous reports. Continuous development in fabrication technologies is the fundamental enabler to realize plasmonic PCF structures and devices with promised functionalities

and performance, which is also the key to drive development of practical applications based on plasmonic PCF devices.

Funding.

Funding support through the AoE schemes (AoE/P-02/12) from the Research Grants Council (RGC) of Hong Kong Special Administrative Region, and through an internal project (4930722) from The Chinese University of Hong Kong are gratefully acknowledged.

Bibliography

[1] J. Homola, "Surface plasmon resonance sensors for detection of chemical and biological species," *Chemical Reviews,* vol. 108, pp. 462-493, 2008.

[2] W. L. Barnes, A. Dereux and T. W. Ebbesen, "Surface plasmon subwavelength optics," *Nature,* vol. 424, pp. 824-830, 2003.

[3] R. C. Jorgenson and S. S. Yee, "A fiber-optic chemical sensor based on surface plasmon resonance," *Sensors and Actuators B,* vol. 12, pp. 213-230, 1993.

[4] R. Slavík, J. Homola and J. Čtyroký, "Single-mode optical fiber surface plasmon resonance sensor," *Sensors and Actuators B: Chemical,* vol. 54, no. 1-2, pp. 74-79, 1999.

[5] W.-H. Lin, Y.-C. Tsai, Y.-C. Tsao and J.-K. Tai, "An enhanced optical multimode fiber sensor based on surface plasmon resonance with cascaded structure," *IEEE Photonics Technology Letters,* vol. 20, no. 15, pp. 1287 - 1289, 2008.

[6] A. Trouillet, C. Ronot-Trioli, C. Veillas and H. Gagnaire, "Chemical sensing by surface plasmon resonance in a multimode optical fibre," *Pure and Applied Optics: Journal of the European Optical Society Part A,* vol. 5, pp. 227-237, 1996.

[7] B.-H. Liu, Y.-X. Jiang, X.-S. Zhu, X.-L. Tang and Y.-W. Shi, "Hollow fiber surface plasmon resonance sensor for the detection of liquid with high refractive index," *Optics Express,* vol. 21, no. 26, pp. 32349-32357, 2013.

[8] R. J. Whelan and R. N. Zare, "Surface Plasmon Resonance Detection for Capillary Electrophoresis Separations," *Analytical Chemistry,* vol. 75, no. 6, pp. 1542-1547, 2003.

[9] R. Jha, R. K. Verma and B. D. Gupta, "Surface plasmon resonance-based tapered fiber optic sensor: sensitivity enhancement by introducing a teflon layer between core and metal layer," *Plasmonics,* vol. 3, pp. 151-156, 2008.

[10] Y.-C. Kim, W. Peng, S. Banerji and K. Booksh, "Tapered fiber optic surface plasmon resonance sensor for analyses of vapor and liquid phases," *Optics Letters,* vol. 30, no. 17, pp. 2218-2220, 2005.

[11] H.-Y. Lin, C.-H. Huang, G.-L. Cheng, N.-K. Chen and H.-C. Chui, "Tapered optical fiber sensor based on localized surface plasmon resonance," *Optics Express,* vol. 20, no. 20, pp. 21693-21701, 2012.

[12] S. K. Srivastava, V. Arora, S. Sapra and B. D. Gupta, "Localized Surface Plasmon Resonance-Based Fiber Optic U-Shaped Biosensor for the Detection of Blood Glucose," *Plasmonics,* vol. 7, pp. 261-268, 2012.

[13] R. K. Verma and B. D. Gupta, "Theoretical modelling of a bi-dimensional U-shaped surface plasmon resonance based fibre optic sensor for sensitivity enhancement," *Journal of Physics D: Applied Physics,* vol. 41, no. 9, p. 095106, 2008.

[14] A. Patnaik, K. Senthilnathan and R. Jha, "Graphene-Based Conducting Metal Oxide Coated D-Shaped Optical Fiber SPR Sensor," *IEEE Photonics Technology Letters,* vol. 27, no. 23, pp. 2437-2440, 2015.

[15] N. Rezaei and A. Yahaghi, "A High Sensitivity Surface Plasmon Resonance D-Shaped Fiber Sensor Based on a Waveguide-Coupled Bimetallic Structure: Modeling and Optimization," *IEEE Sensors Journal,* vol. 14, no. 10, pp. 3611-3615, 2014.

[16] H.-Y. Lin, W.-H. Tsai, Y.-C. Tsao and B.-C. Sheu, "Side-polished multimode fiber biosensor based on surface plasmon resonance with halogen light," *Applied Optics,* vol. 46, no. 5, pp. 800-806, 2007.

[17] H.-Y. Lin, Y.-C. Tsao, W.-H. Tsai, Y.-W. Yang, T.-R. Yan and B.-C. Sheu, "Development and application of side-polished fiber immunosensor based on surface plasmon resonance for the detection of Legionella pneumophila with halogens light and 850 nm-LED," *Sensors and Actuators A,* vol. 138, pp. 299-305, 2007.

[18] T.-J. Lin and C.-T. Lou, "Reflection-based localized surface plasmon resonance fiber-optic probe for chemical and biochemical sensing at high-pressure conditions," *The Journal of Supercritical Fluids,* vol. 41, no. 2, pp. 317-325, 2007.

[19] Y. Lin, Y. Zou and R. G. Lindquist, "A reflection-based localized surface plasmon resonance fiber-optic

probe for biochemical sensing," *Biomedical Optics Express,* vol. 2, no. 3, pp. 478-484, 2011.

[20] L.-Y. Shao, Y. Shevchenko and J. Albert, "Intrinsic temperature sensitivity of tilted fiber Bragg grating based surface plasmon resonance sensors," *Optics Express,* vol. 18, no. 11, pp. 11464-11471, 2010.

[21] C. Shen, Y. Zhang, W. Zhou and J. Albert, "Au-coated tilted fiber Bragg grating twist sensor based on surface plasmon resonance," *Applied Physics Letters,* vol. 104, p. 071106, 2014.

[22] T. Schuster, R. Herschel, N. Neumann and C. G. Schäffer, "Miniaturized Long-Period Fiber Grating Assisted Surface Plasmon Resonance Sensor," *Journal of Lightwave Technology,* vol. 30, no. 8, pp. 1003-1008, 2012.

[23] Y. J. He, "Investigation of LPG-SPR sensors using the finite element method and eigenmode expansion method," *Optics Express,* vol. 21, no. 12, pp. 13875-13895, 2013.

[24] J. C. Knight, "Photonic crystal fibres," *Nature,* pp. 847-851, 2003.

[25] P. Russell, "Photonic Crystal Fibers," *Science,* pp. 358-362, 2003.

[26] J. Villatoro and J. Zubia, "New perspectives in photonic crystal fibre sensors," *Optics & Laser Technology,* pp. 67-75, 2016.

[27] Y. Zhao, Z. Deng and J. Li, "Photonic crystal fiber based surface plasmon resonance chemical sensors," *Sensors and Actuators B,* vol. 202, pp. 557-567, 2014.

[28] B. D. Gupta and R. K. Verma, "Surface plasmon resonance-based fiber optic sensors:," *Journal of Sensors,* p. 979761, 2009.

[29] A. K. Sharma, R. Jha and B. D. Gupta, "Fiber-Optic Sensors Based on Surface Plasmon Resonance: A Comprehensive Review," *IEEE Sensors Journal,* vol. 7, pp. 1118-1129, 2007.

[30] X. Yang, C. Gu, F. Qian, Y. Li and J. Z. Zhang, "Highly Sensitive Detection of Proteins and Bacteria in Aqueous Solution Using Surface-Enhanced Raman Scattering and Optical Fibers," *Analytical Chemistry,* vol. 83, pp. 5888-5894, 2011.

[31] A. Urrutia, J. Goicoechea and F. J. Arregui, "Optical Fiber Sensors Based on Nanopartical-Embedded Coatings," *Journal of Sensors,* p. 805053, 2015.

[32] C. Caucheteur, T. Guo and J. Albert, "Review of plasmonic fiber optic biochemical sensors: improving the limit of detection," *Analytical and Bioanalytical Chemistry,* vol. 407, no. 14, p. 3883–3897, 2015.

[33] E. Kretschmann and H. Z. Raether, "Radiative decay of non radiative surface plasmons excited by light," *Naturforsch A,* vol. 23, no. 12, p. 2135, 1968.

[34] M.-H. Chiu, C.-H. Shih and M.-H. Chi, "Optimum sensitivity of single-mode D-typte optical fiber sensor in the intensity measurement," *Sensors and Actuators B,* vol. 123, no. 2, p. 1120, 2007.

[35] L. Coelho, J. M. M. M. de Almeida, J. L. Santos, R. A. S. Ferreira, P. S. André and D. Viegas, "Sensing structure based on surface plasmon resonance in chemically etched single mode optical fibres," *Plasmonics,* vol. 10, no. 2, p. 319, 2015.

[36] M. Born and E. Wolf, Principles of Optics, 7th edition ed., Cambidge: Cambridge Univeristy Press, 1999, pp. 752-758.

[37] P. Yeh, Optical waves in layered media, New York: John Wiley & Sons., 1998.

[38] A. Nagasaki, K. Saitoh and M. Koshiba, "Polarization characteristics of photonic crystal fibers selectively filled with metal wires into cladding air holes," *Optics Express,* vol. 19, no. 4, pp. 3799-3808, 2011.

[39] J. N. Dash and R. Jha, "SPR biosensor based on polymer PCF coated with conducting metal oxide," *IEEE Photonics Technology Letters,* vol. 26, no. 6, pp. 594-598, 2014.

[40] C. Sauvan, J. P. Hugonin, I. S. Maksymov and P. Lalanne, "Theory of the spontaneous optical emission of nanosize photonic and plasmonic resonators," *Physics Review Letters,* vol. 110, p. 237401, 2013.

[41] M. Sun, Y. Wang, Z. N. Chen, Y. Gong, J. Lim and X. Qing, "Nanostars on a fiber facet with near field enhancement for surface-enhanced Raman scattering detection," *Applied Physics A: Materials Science & Processing,* vol. 115, no. 1, pp. 87-91, 2014.

[42] J. Hou, D. Bird, A. George, S. Maier, B. T. Kuhlmey and J. C. Knight, "Metallic mode confinement in microstructured fibres," *Optics Express,* vol. 16, no. 9, pp. 5983-5990, 2008.

[43] A. Tuniz, B. T. Kuhlmey, R. Lwin, A. Wang, J. Anthony, R. Leonhardt and S. C. Fleming, "Drawn metamaterials with plasmonic response at terahertz frequencies," *Applied Physics Letters,* vol. 96, p. 191101, 2010.

[44] C. E. Finlayson, A. Amezcua-Correa and P. J. A. Sazio, "Electrical and Raman characterization of silicon and germanium-filled microstrcutred optical fibers," *Applied Physics Letters,* vol. 90, p. 132110, 2007.

[45] M. A. Schmidt, L. N. P. Sempere, H. K. Tyagi, C. G. Poulton and P. S. J. Russell, "Waveguiding and plasmon resonances in two-dimensional photonic lattices of gold and silver nanowires," *Physical Review B,* vol. 77, no. 3, p. 033417, 2008.

[46] H. W. Lee, M. A. Schmidt, H. K. Tyagi, L. P. Sempere and P. S. J. Russel, "Polarization-dependent coupling

to plasmon modes on submicron gold wire in photonic crystal fiber," *Applied Physics Letters,* vol. 93, p. 111102, 2008.

[47] H. W. Lee, M. A. Schmidt, R. F. Russel, N. Y. Joly, H. K. Tyagi, P. Uebel and P. S. J. Russell, "Pressure-assisted melt-filling and optical characterization of Au nano-wires in microstructured fibers," *Optics Express,* vol. 19, no. 13, pp. 12180-12189, 2011.

[48] I. W. Donald and B. L. Metcalfe, "The preparation, properties and applications of some glass-coated metal filaments prepared by the Taylor-wire process," *J. Mater. Sci,* vol. 31, pp. 1139-1149, 1996.

[49] X. Zhang, Z. Ma, Z.-Y. Yuan and M. Su, "Mass-productions of vertically aligned extremely long metallic micro/nanowires using fiber drawing nanomanufacturing," *Advanced Materials,* vol. 20, pp. 1310-1314, 2008.

[50] M. Yaman, T. Khudiyev, E. Ozgur, M. Kanik, O. Aktas, E. O. Ozgur, H. Deniz, E. Korkut and M. Bayindir, "Arrays of indefinitely long uniform nanowires and nanotubes," *Nature Materials,* vol. 10, pp. 494-501, 2011.

[51] H. Tyagi, H. W. Lee, P. Uebel, M. A. Schmidt, N. Joly, M. Scharrer and P. S. J. Russell, "Plasmon resonances on gold nanowires directly," *Optics Letters,* vol. 35, no. 15, pp. 2573-2575, 2010.

[52] A. Witkowska, K. Lai, S. G. Leon-Saval, W. J. Wadsworth and T. A. Birks, "All-fiber anamorphic core-shape transitions," *Optics Letters,* vol. 31, no. 18, pp. 2672-2674, 2006.

[53] P. Uebel, M. A. Schmidt, H. W. Lee and P. S. J. Russell, "Polarisation-resolved near-field mapping of a coupled gold nanowire array," *Optics Express,* vol. 20, no. 27, pp. 28409-28417, 2012.

[54] H. W. Lee, M. A. Schmidt and P. S. J. Russell, "Excitation of a nanowire “molecule” in gold-filled photonic crystal fiber," *Optics Letter,* vol. 37, no. 14, pp. 2946-2948, 2012.

[55] C. Jain, A. Tuniz, K. Reuther, T. Wieduwilt, M. Rettenmayr and M. A. Schmidt, "Micron-sized gold-nickel alloy wire integrated silica optical fibers," *Optics Express,* vol. 6, no. 6, pp. 1790-1799, 2016.

[56] Y. Lu, M. T. Wang, C. J. Hao, Z. Q. Zhao and J. Q. Yao, "Temperature sensing using photonic crystal fiber filled with silver nanowires and liquid," *IEEE Photonics Journal,* vol. 6, no. 3, p. 680137, 2014.

[57] X. C. Yang, Y. Lu, B. L. Liu and J. Q. Yao, "Temperature sensor based on photonic crystal fiber filled with liquid and silver nanowires," *IEEE Photonics Journal,* vol. 8, no. 3, p. 6803309, 2016.

[58] P. J. A. Sazio, A. Amezcua-Correa, C. E. Finlayson, J. R. Hayes, T. J. Scheidemantel, N. F. Baril, B. R. Jackson, D. J. Won, F. Zhang, E. R. Margine, V. Gopolan, V. H. Crespi and J. V. Badding, "Microstructured Optical Fibers as High-Pressure Microfluidic Reactors," *Science,* vol. 311, pp. 1583-1586, 2006.

[59] J. Boehm, A. Francois, H. Ebendorff-Heidepriem and T. M. Monro, "Chemical deposition of silver for the fabrication of surface plasmon microstructured optical fibre sensors," *Plasmonics,* vol. 6, pp. 133-136, 2011.

[60] X. Zhang, R. Wang, F. M. Cox, B. T. Kuhlmey and M. C. J. Large, "Selective coating of holes in microstructured optical fiber and its application to in-fiber absorptive polarizers," *Optics Express,* vol. 15, no. 24, pp. 16270-16278, 2007.

[61] E. Klantsataya, A. Francois, H. Ebendorff-Heidepriem, P. Hoffmann and T. M. Monro, "Surface plasmon scattering in exposed core optical fiber for enhanced resolution refractive index sensing," *Sensors,* vol. 15, pp. 25090-25012, 2015.

[62] A. Wang, A. Docherty, B. T. Kuhlmey, F. M. Cox and M. C. J. Large, "Side-hole fiber sensor based on surface plasmon resonance," *Optics Letters,* vol. 34, no. 24, pp. 3890-3892, 2009.

[63] X. Yu, D. Yong, H. Zhang, H. Li, Y. Zhang, C. C. Chan, H.-P. Ho, H. Liu and D. Liu, "Plasmonic enhanced fluorescence spectroscopy using side-polished microstructured optical fiber," *Sensors and Actuators B: Chemical,* vol. 160, no. 1, pp. 196-201, 2011.

[64] D. J. J. Hu, J. L. Lim, M. K. Park, L. T. H. Kao, Y. Wang, H. Wei and W. Tong, "Photonic crystal fiber-based interferometric biosensor for streptavidin and biotin detection," *IEEE Journal of Selected Topics in Quantum Electronics,* vol. 18, no. 4, pp. 1293-1297, 2012.

[65] D. J. J. Hu, J. L. Lim, M. Jiang, Y. Wang, F. Luan, P. P. Shum, H. Wei and W. Tong, "Long period grating cascaded to photonic crystal fiber modal interferometer for simultaneous measurement of temperature and refractive index," *Optics Letters,* vol. 37, no. 12, pp. 2283-2285, 2012.

[66] W. C. Wong, C. C. Chan, J. L. Boo, Z. Y. Teo, Z. Q. Tou, H. B. Yang, C. M. Li and K. C. Leong, "Photonic Crystal Fiber Surface Plasmon Resonance Biosensor Based on Protein G Immobilization," *IEEE Journal of Selected Topics in Quantum Electronics,* vol. 19, no. 3, p. 460217, 2013.

[67] H. E. Arabi, M. Pournoury, J. H. Park, S. Im and K. Oh, "Plamonically enhanced optical transmission through a metalized nanostructured photonic crystal fiber taper," *Optics Letters,* vol. 36, no. 11, pp. 2029-2031, 2011.

[68] T. K. Sau and C. J. Murphy, "Self-Assembly Patterns Formed upon Solvent Evaporation of Aqueous Cetyltrimethylammonium Bromide-Coated Gold Nanoparticles of Various Shapes," *Langmuir,* vol. 21, no. 7, pp. 2923-2929, 2005.

[69] H. Yan, J. Liu, C. Yang, G. Jin, C. Gu and L. Hou, "Novel index-guided photonic crystal fiber surface-enhanced Raman scattering probe," *Optics Express,* vol. 16, no. 11, pp. 8300-8305, 2008.

[70] Z. Xie, Y. Lu, H. Wei, J. Yan, P. Wang and H. Ming, "Broad spectral photonic crystal fiber surface enhanced Raman scattering probe," *Applied Physics B,* vol. 95, pp. 751-755, 2009.

[71] N. Zhang, G. Humbert, T. Gong, P. P. Shum, K. Li, J. -L. Auguste, Z. Wu, D. J. J. Hu, F. Luan, Q. X. Dinh, M. Olivo and L. Wei, "Side-channel photonic crystal fiber for surface enhanced Raman scattering sensing," *Sensors and Actuators B: Chemical,* vol. 223, pp. 195-201, 2016.

[72] H. Yan, C. Gu, C. Yang, J. Liu, G. Jin, J. Zhao, L. Hou and Y. Yao, "Hollow core photonic crystal fiber surface-enhanced Raman probe," *Applied Physics Letters,* vol. 89, p. 204101, 2006.

[73] F. M. Cox, A. Argyros, M. C. J. Large and S. Kalluri, "Surface enhanced Raman scattering in a hollow core microstructured optical fiber," *Optics Express,* vol. 15, no. 21, pp. 13675-13681, 2007.

[74] Y. Han, S. Tan, M. K. K. Oo, D. Pristinski, S. Sukhishvili and H. Du, "Towards full-length accumulative surface-enhanced Raman scattering-active photonic crystal fibers," *Advanced Materials,* vol. 22, pp. 2647-2651, 2010.

[75] V. S. Tiwari, A. Khetani, A. Momenpour and H. Anis, "Optimum size and volume of nanoparticle within hollow core photonic crystal fiber," *IEEE Journal of Selected Topics in Quantum Electronics,* vol. 20, no. 3, p. 7300608, 2014.

[76] Y. Zhang, C. Shi, C. Gu, L. Seballos and J. Z. Zhang, "Liquid core photonic crystal fiber sensor based on surface enhanced Raman scattering," *Applied Physics Letters,* vol. 90, no. 19, p. 193504, 2007.

[77] J. Irizar, J. Dinglasan, J. B. Goh, A. Khetani, H. Anis, D. Anderson, C. Goh and A. S. Helmy, "Raman spectroscopy of nanoparticles using hollow-core photonic crystal fibers," *IEEE Journal of Selected Topics in Quantum Electronics,* vol. 14, no. 4, pp. 1214-1222, 2008.

[78] X. Yang, C. Shi, D. Wheeler, R. Newhouse, B. Chen, J. Z. Zhang and C. Gu, "High-sensitivity molecular sensing using hollow-core photonic crystal fiber and surface-enhanced Raman scattering," *Journal of the Optical Society of America A,* vol. 27, no. 5, pp. 977-984, 2010.

[79] C. Shi, C. Lu, C. Gu, L. Tian, R. Newhouse, S. Chen and J. Z. Zhang, "Inner wall coated hollow core waveguide sensor based on double substrate surface enhanced Raman scattering," *Applied Physics Letters,* vol. 93, p. 153101, 2008.

[80] X. Yang, C. Shi, R. Newhouse, J. Z. Zhang and C. Gu, "Hollow-core Photonic Crystal Fibers for Surface-Enhanced Raman Scattering Probes," *International Journal of Optics,* vol. 2011, p. 751610, 2010.

[81] M. K. K. Oo, Y. Han, J. Kanka, S. Sukhishvili and H. Du, "Structure fits the purpose: photonic crystal fibers for evanescent field surface enhanced raman spectroscopy," *Optics Letters,* vol. 35, no. 4, pp. 466-468, 2010.

[82] M. K. K. Oo, Y. Han, R. Martini, S. Sukhishvili and H. Du, "Forward-propagating surface-enhanced Raman scattering and intensity distribution in photonic crystal fiber with immobilized Ag nanoparticles," *Optics Letters,* vol. 34, no. 7, pp. 968-970, 2009.

[83] Y. Zhang, D. Yong, X. Yu, L. Xia, D. Liu and Y. Zhang, "Amplification of Surface-Enhance Raman Scattering in Photonic Crystal Fiber Using Offset Launch Method," *Plasmonics,* vol. 8, pp. 209-215, 2013.

[84] A. Khetani, J. Riordon, V. Tiwari, A. Momenpour, M. Godin and H. Anis, "Hollow core photonic crystal fiber as a reusable Raman biosensor," *Optics Express,* vol. 21, no. 10, pp. 12340-12350, 2013.

[85] A. Csaki, F. Jahn, I. Latka, T. Henkel, D. Malsch, T. Schneider, K. Schroder, K. Schuster, A. Schwuchow, R. Spittel, D. Zopf and W. Fritzsche, "Nanoparticle layer deposition for plasmonic tuning of microstructured optical fibers," *Small,* vol. 6, no. 22, pp. 2584-2589, 2010.

[86] K. Schröder, A. Csáki, A. Schwuchow, F. Jahn, K. Strelau, I. Latka, T. Henkel, D. Malsch, K. Schuster, K. Weber, T. Schneider, R. Möller and W. Fritzsche, "Functionalization of Microstructured Optical Fibers by Internal Nanoparticle Mono-Layers for Plasmonic Biosensor Applications," *IEEE Sensors Journal,* vol. 12, no. 1, pp. 218-224, 2012.

[87] A. Amezcua-Correa, J. Yang, C. E. Finlayson, A. C. Peacor, J. Hayes, P. Sazio, J. J. Baumberg and S. M. Howdle, "Surface-enhanced Raman scattering using microstructured optical fiber substrates," *Advanced Functional Materials,* vol. 17, pp. 2024-2030, 2007.

[88] A. C. Peacock, A. Amezcua-Correa, J. Yang, P. J. A. Sazio and S. M. Howdle, "Highly efficient surface enhanced Raman scattering using microstructured optical fibers with enhanced plasmonic interactions," *Applied Physics Letters,* vol. 92, p. 114113, 2008.

[89] L. Bigot, H. E. Hamzaoui, A. L. Rouge, G. Bouwmans, F. Chassagneux, B. Capoen and M. Bouazaoui, "Linear and nonlinear optical properties of gold nanoparticle-doped photonic crystal fiber," *Optics Express,* vol. 19, no. 20, pp. 19061-19066, 2011.

[90] U. S. Dinish, C. Y. Fu, K. S. Soh, R. Bhuvaneswari, A. Kumar and M. Olivo, "Highly sensitive SERS detection of cancer proteins in low sample volume using hollow core photonic crystal fiber," *Biosensors and Bioelectronics,* vol. 33, pp. 293-298, 2012.

[91] U. S. Dinish, G. Balasundara, Y. T. Chang and M. Olivo, "Sensitive multiplex detection of serological liver cancer biomarkers using SERS-active photonic crystal fiber probe," *Journal of Biophotonics,* vol. 7, no. 11-12, pp. 956-965, 2014.

[92] A. Khetani, A. Momenpour, E. I. Alarcon and H. Anis, "Hollow core photonic crystal fiber for monitoring leukemia cells using surface enhanced Raman scattering (SERS)," *Optics Express,* vol. 23, no. 22, pp. 4599-4609, 2015.

[93] T. Gong, Y. Cui, D. Goh, K. K. Voon, P. P. Shum, G. Humbert, J.-L. Auguste, X.-Q. Dinh, K.-T. Yong and M. Olivo, "Highly sensitive SERS detection and quantification of sialic acid on single cell using photonic-crystal fiber with gold nanoparticles," *Biosensors and Bioelectronics,* vol. 64, pp. 227-233, 2015.

[94] P. Pinkhasova, H. Chen, J. Kanka, P. Mergo and H. Du, "Nanotag-enabled photonic crystal fiber as quantitative surface-enhanced Raman scattering optofluidic platform," *Applied Physics Letters,* vol. 106, p. 071106, 2015.

[95] A. Hassani and M. Skorobogatiy, "Design of the microstructured optical fiber-based surface plasmon resonance sensors with enhanced microfluidics," *Optics Express,* vol. 14, no. 24, pp. 11616-11621, 2006.

[96] A. Hassani and M. Skorobogatiy, "Design criteria for microstructured-optical-fiber-based surface-plasmon-resonance sensors," *Journal of the Optical Society of America B,* vol. 24, no. 6, pp. 1423-1429, 2007.

[97] L. Zheng, X. Zhang, R. X., J. Gao, L. Shi, X. Liu, Q. Wang and Y. Huang, "Surface plasmon resonance sensors based on Ag-metalized nanolayer in microstructured optical fibers," *Optics & Laser Technology,* vol. 43, pp. 960-964, 2011.

[98] X. Yu, Y. Zhang, S. Pan, P. Shum, M. Yan, Y. Leviatan and C. Li, "A selectively coated photonic crystal fiber based surface plasmon resonance sensor," *Journal of Optics,* vol. 12, no. 1, p. 015005, 2010.

[99] W. Wei, X. Zhang, X. Guo, L. Zheng, J. Gao, W. Shi, Q. Wang, Y. Huang and X. Ren, "Refractive index sensors based on Ag-metalized nanolayer in microstructured optical fibers," *Optik,* vol. 123, pp. 1167-1170, 2012.

[100] E. K. Akowuah, T. Gorman, H. Ademgil, S. Haxha, G. K. Robinson and J. V. Oliver, "Numerical analysis of a photonic crystal fiber for biosensing applications," *IEEE Journal of Quantum Electronics,* vol. 48, no. 11, pp. 1403-1409, 2012.

[101] S. I. Azzam, M. F. O. Hameed, R. E. A. Shehata, A. M. Heikal and S. S. A. Obayya, "Multichannel photonic crystal fiber surface plasmon resonance based sensor," *Optical and Quantum Electronics,* vol. 48, p. 142, 2016.

[102] Y. Lu, C.-J. Hao, B.-Q. Wu, M. Musideke, L.-C. Duan, W.-Q. Wen and J.-Q. Yao, "Surface plasmon resonance sensor based on polymer photonic crystal fibers with metal nanolayers," *Sensors,* vol. 13, pp. 956-965, 2013.

[103] R. Otupiri, S. K. Akowuah, S. Haxha, H. Ademgil, A. F. and A. Aggoun, "A Novel Birefringent Photonic Crystal Fiber Surface Plasmon Resonance Biosensor," *IEEE Photonis Journal,* vol. 6, no. 4, p. 6801711, 2014.

[104] A. A. Rifat, G. A. Mahdiraji, Y. M. Sua, Y. G. Shee, R. Ahmed, D. M. Chow and F. R. M. Adikan, "Surface Plasmon Resonance Photonic Crystal Fiber Biosensor: A Practical Sensing Approach," *IEEE Photonics Technology Letters ,* vol. 27, no. 15, pp. 1628-1631, 2015.

[105] M. F. O. Hameed, Y. K. A. Alrayk and S. S. A. Obayya, "Self-calibration highly sensitive photonic crystal fiber biosensor," *IEEE Photonics Journal,* vol. 8, no. 3, p. 6802912, 2016.

[106] N. Luan, R. Wang, W. Lv and J. Yao, "Surface plasmon resonance sensor based on D-shaped microstructured optical fiber with hollow core," *Optics Express,* vol. 23, no. 7, pp. 8576-8582, 2015.

[107] C. Zhou, Y. Zhang, L. Xia and D. Liu, "Photonic crystal fiber sensor based on hybrid mechanisms: Plasmonic and directional," *Optics Communications,* vol. 285, pp. 2466-2471, 2012.

[108] G. An, S. Li, X. Yan, X. Zhang, Z. Yuan, H. Wang, Y. Zhang, X. Hao, Y. Shao and Z. Hao, "Extra-broad photonic crystal fiber refractive index sensor based on surface plasmon resonance," *Plasmonics,* 2016.

[109] D. Gao, C. Guan, Y. Wen, X. Zhong and L. Yuan, "Multi-hole fiber based surface plasmon resonance sensor operated at near-infrared wavelengths," *Optics Communications,* vol. 313, pp. 94-98, 2014.

[110] M. Napiorkowski and W. Urbanczyk, "Effect of bending on surface plasmon resonance spectrum in microstructured optical fibers," *Optics Express,* vol. 21, no. 19, pp. 22762-22772, 2013.

[111] M. Hautakorpi, M. Mattinen and H. Ludvigsen, "Surface-plasmon-resonance sensor based on three-hole microstructured optical fiber," *Optics Express,* vol. 16, no. 12, pp. 8427-8432, 2008.

[112] Y. Lu, C.-J. Hao, B.-Q. Wu, X.-H. Huang, W.-Q. Wen, X.-Y. Fu and J.-Q. Yao, "Grapefruit fiber filled with silver nanowires surface plasmon resonance sensor in aqueous environments," *Sensors,* vol. 12, pp. 12016-12025, 2012.

[113] X. Yang, Y. Lu, M. Wang and J. Yao, "An Exposed-Core Grapefruit Fibers Based Surface Plasmon Resonance Sensor," *Sensors,* vol. 15, pp. 17106-17114, 2015.

[114] N. Luan and J. Yao, "Surface Plasmon Resonance Sensor Based On Exposed-Core Microstructured Optical Fiber Placed with A Silver Wire," *IEEE Photonics Journal,* vol. 8, no. 1, p. 4800508, 2016.

[115] C. J. Hao, Y. Lu, M. T. Wang, B. Q. Wu, L. C. Duan and J. Q. Yao, "Surface plasmon resonance refractive index sensor based on active photonic crystal fiber," *IEEE Photonics Journal,* vol. 5, no. 6, p. 4801108, 2013.

[116] G. An, S. Li, W. Qin, W. Zhang, Z. Fan and Y. Bao, "High-sensitivity refractive index sensor based on D-shaped photonic crystal fiber with rectangular lattice and nanoscale gold film," *Plasmonics,* vol. 9, pp. 1355-1360, 2014.

[117] G. Wang, S. Li, G. An, X. Wang, Y. Zhao, W. Zhang and H. Chen, "Highly sensitive D-shaped photonic crystal fiber biological sensors based on surface plasmon resonance," *Optical and Quantum Electronics,* vol. 48, p. 46, 2016.

[118] L. Peng, F. Shi, G. Zhou, S. Ge, Z. Hou and C. Xia, "A Surface Plasmon Biosensor Based on a D-Shaped Microstructured Optical Fiber With Rectangular Lattice," *IEEE Photonics Journal,* vol. 7, no. 5, p. 4801309, 2015.

[119] Z. Tan, X. Hao, Y. Shao, Y. Chen, X. Li and P. Fan, "Phase modulation and structural effects in a D-shaped all-solid photonic crystal fiber surface plasmon resonance sensor," *Optics Express,* vol. 22, no. 12, pp. 15049-15063, 2014.

[120] F. Shi, L. Peng, G. Zhou, X. Cang, Z. Hou and C. Xia, "An Elliptical Core D-Shaped Photonic Crystal Fiber-Based Plasmonic Sensor at Upper Detection Limit," *Plasmonics,* vol. 10, no. 6, pp. 1263-1268, 2015.

[121] J. N. Dash and R. Jha, "Highly sensitive D shaped PCF sensor based on SPR for near IR," *Optical and Quantum Electronics,* vol. 48, p. 137, 2016.

[122] J. N. Dash and R. Jha, "Highly sensitive side-polished birefringent PCF-based SPR sensor in near IR," *Plasmonics,* 2016.

[123] T. Huang, "Highly sensitive SPR sensor based on D-shaped photonic crystal fiber coated with Indium Tin oxide at near-infrared wavelength," *Plasmonics,* 2016.

[124] N. M. Y. Zhang, D. J. J. Hu, P. P. Shum, Z. Wu, K. Li, T. Huang and L. Wei, "Design and analysis of surface plasmon resonance sensor based on high birefringent microstructured optical fiber," *Journal of Optics,* vol. 18, p. 065005, 2016.

[125] X. Yu, S. Zhang, Y. Zhang, H.-P. Ho, P. Shum, H. Liu and D. Liu, "An efficient approach for investigating surface plasmon resonance in asymmetric optical fibers based on birefringence analysis," *Optics Express,* vol. 18, no. 17, pp. 17950-17957, 2010.

[126] C. Liu, F. Wang, S. Zheng, T. Sun, J. Lv, Q. Liu, L. Yang, H. Mu and P. K. Chu, "Analysis of a highly birefringent asymmetric photonic crystal fibre based on a surface plasmon resonance sensor," *Journal of Modern Optcis,* pp. 1189-1195, 2016.

[127] S. Ge, F. Shi, G. Zhou, S. Liu, Z. Hou and L. Peng, "U-shaped photonic crystal fiber based surface plasmon resonance sensors," *Plasmonics,* 2016.

[128] J. N. Dash and R. Jha, "Graphene-based birefringent photonic crystal fiber sensor using surface plasmon resonance," *IEEE Photonics Technology Letters,* vol. 26, no. 11, pp. 1092-1095, 2014.

[129] J. N. Dash and R. Jha, "On the performance of graphene-based D-shaped photonic crystal fibre biosensor using surface plasmon resonance," *Plasmonics,* vol. 10, no. 5, pp. 1123-1131, 2015.

[130] A. A. Rifat, G. A. Mahdiragi, D. M. Chow, Y. G. Shee, R. Ahmed and F. R. M. Adikan, "Photonic crystal fiber-based surface plasmon resonance sensor with selective analyte channels and graphene-silver deposited core," *Sensors,* vol. 15, pp. 11499-11410, 2015.

[131] X. Yang, Y. Lu, B. Liu and J. Yao, "Analysis of Graphene-Based Photonic Crystal Fiber Sensor Using Birefringence and Surface Plasmon Resonance," *Plasmonics,* pp. 1-8, 2016.

[132] A. A. Rifat, G. A. Mahdiraji, R. Ahmed, D. M. Chow, Y. M. Sua, Y. G. Shee and F. R. M. Adikan, "Copper-Graphene-based photonic crystal fiber plasmonics biosensor," *IEEE Photonics Journal,* vol. 8, no. 1, p. 4800408, 2016.

[133] Y. Zhang, L. Xia, C. Zhou, X. Yu, H. Liu, D. Liu and Y. Zhang, "Microstructured fiber based plasmonic index sensor with optimized accuracy and calibration relation in large dynamic range," *Optics Communications,* vol. 284, pp. 4161-4166, 2011.

[134] B. Shuai, L. Xia, Y. Zhang and D. Liu, "A multi-core holey fiber based plasmonic sensor with large detection range and high linearity," *Optics Express,* vol. 20, no. 6, pp. 5974-5968, 2012.

[135] C. Liu, F. Wang, J. Lv, T. Sun, Q. Liu, H. Mu and P. K. Chu, "Design and theoretical analysis of a photonic crystal fiber based on surface plasmon resonance sensing," *Journal of Nanophotonics,* vol. 9, p. 093050, 2015.

[136] B. Shuai, L. Xia and D. Liu, "Coexistence of positive and negative refractive index sensitivity in the liquid-core photonic crystal fiber based plasmonic sensor," *Optics Express,* vol. 20, no. 23, pp. 25858-25866, 2012.

[137] W. Qin, S. Li, Y. Yao, X. Xin and J. Xue, "Analyte-filled core self-calibration microstructured optical fiber based plasmonic sensor for detecting high refractive index aqueous analyte," *Optics and Lasers in Engineering,* vol. 58, pp. 1-8, 2014.

[138] M. S. A. Gandhi, S. Sivabalan, P. R. Babu and K. Senthilnathan, "Designing a biosensor using a photonic quasi-crystal Fiber," *IEEE Sensors Journal,* vol. 16, no. 8, pp. 2425-2430, 2016.

[139] Z. Fan, S. Li, Q. Liu, G. An, H. Chen, J. Li, D. Chao, H. Li, J. Zi and W. Tian, "High sensitivity of refractive index sensor based on analyte-filled photonic crystal fiber with surface plasmon resonance," *IEEE Photonics Journal,* vol. 7, no. 3, p. 4800809, 2015.

[140] Z. Tan, X. Li, Y. Chen and P. Fan, "Improving the Sensitivity of Fiber Surface Plasmon Resonance Sensor by Filling Liquid in a Hollow Core Photonic Crystal Fiber," *Plasmonics,* vol. 9, no. 1, pp. 167-173, 2014.

[141] B. Gauvreau, A. Hassani, M. F. Fehri, A. Kabashin and M. Skorobogatiy, "Photonic bandgap fiber-based Surface Plasmon Resonance Sensors," *Optics Express,* vol. 15, no. 18, pp. 11413-11426, 2007.

[142] A. Hassani, B. Gauvreau, M. F. Fehri, A. Kabashin and M. Skorobogatiy, "Photonic crystal fiber and waveguide-based surface plasmon resonance sensors for application in the visible and near-IR," *Electromagnetics,* vol. 28, no. 3, pp. 198-213, 2008.

[143] M. Tian, P. Lu, L. Chen, C. Lv and D. Liu, "All-solid D-shaped photonic fiber sensor based on surface plasmon resonance," *Optics Communications,* vol. 285, pp. 1550-1554, 2012.

[144] Y. Zhang, C. Zhou, L. Xia, X. Yu and D. Liu, "Wagon wheel fiber based multichannel plasmonic sensor," *Optics Express,* vol. 19, no. 23, pp. 22863-22873, 2011.

[145] R. Otupiri, E. K. Akowuah and S. Haxha, "Multi-channel SPR biosensor based on PCF for multi-analyte sensing applications," *Optics Express,* vol. 23, no. 12, pp. 15716-15727, 2015.

[146] N. J. Florous, K. Saitoh and M. Koshiba, "Numerical modeling of cryogenic temperature sensors based on plasmonic oscillations in metallic nanoparticles embeded into photonic crystal fibers," *IEEE Photonics Technology Letters,* vol. 19, no. 5, pp. 324-326, 2007.

[147] N. Luan, R. Wang, W. Lv, Y. Lu and J. Yao, "Surface Plasmon Resonance Temperature Sensor Based on Photonic Crystal Fibers Randomly Filled with Silver Nanowires," *Sensors,* vol. 14, pp. 16035-16045, 2014.

[148] M. Wang, Y. Lu, C. Hao, X. Yang and J. Yao, "Simulation analysis of a temperature sensor based on photonic crystal fiber filled with different shapes of nanowires," *Optik,* vol. 126, pp. 3687-3691, 2015.

[149] Y. Peng, J. Hou, Z. Huang and Q. Li, "Temperature sensor based on surface plasmon resonance within selective coated photonic crystal fiber," *Applied Optics,* vol. 51, no. 26, pp. 6361-6367, 2012.

[150] Q. Liu, S. Li, H. Chen, J. Li and Z. Fan, "High-sensitivity plasmonic temperature sensor based on photonic crystal fiber coated with nanoscale gold film," *Applied Physics Express,* vol. 8, p. 046701, 2015.

[151] D. Hu, J. Lim, Y. Cui, K. Milenko, Y. Wang, P. Shum and T. Wolinski, "Fabrication and characterization of a highly temperature sensitive device based on nematic liquid crystal-filled photonic crystal fiber," *IEEE Photonics Journal,* vol. 4, no. 5, pp. 1248-1255, 2012.

[152] D. Hu, P. Shum, Y. Cui, K. Milenko, Y. Wang and T. Wolinski, "A compact and temperature-sensitive directional coupler based on photonic crystal fiber filled with liquid crystal 6CHBT," *IEEE Photonics Journal,* vol. 4, no. 5, pp. 2010-2016, 2012.

[153] M. F. O. Hameed, M. Y. Azab, A. M. Heikal, S. M. El-Hefnawy and S. S. A. Obayya, "Highly sensitive plasmonic photonic crystal temperature sensor filled with liquid crystal," *IEEE Photonics Technology Letters,* vol. 28, no. 1, pp. 59-62, 2016.

[154] N. Luan, C. Ding and J. Yao, "A refractive index and temperature sensor based on surface plasmon resonance in an exposed-core microstructured optical fiber," *IEEE Photonics Journal,* vol. 8, no. 2, p. 4801608, 2016.

[155] J. Li, S. Wu, S. Brugioni, R. Meucci and S. Faetti, "Infrared refractive indices of liquid crystals," *Journal of Applied Physics,* vol. 97, no. 7, p. 073501, 2005.

[156] Y. Du, S.-G. Li, S. Liu, X.-P. Zhu and X.-X. Zhang, " Polarization splitting filter characteristics of Au-filled high-birefringence photonic crystal fiber," *Applied Physics B,* vol. 109, no. 1, pp. 65-74, 2012.

[157] Z. Fan, S. Li, H. Chen, Q. Liu, W. Zhang, G. An, J. Li and Y. Bao, "Numerical analysis of polarization filter characteristics of D-shaped photonic crystal fiber based on surface plasmon resonance," *Plasmonics,* vol. 10, no. 3, pp. 675-680, 2015.

[158] S. Yogalakshmi, S. Selvendran and A. S. Raja, "Design and analysis of a photonic crystal fiber based polarization filter using surface plasmon resonance," *Laser Physics,* vol. 26, p. 056201, 2016.

[159] F. Shi, G. Zhou, D. Li, L. Peng, Z. Hou and C. Xia, "Surface plasmon mode coupling in photonic crystal fiber symmetrically filled with Ag/Au alloy wires," *Plasmonics,* vol. 10, no. 2, pp. 335-340, 2015.

[160] H. Chen, S. Li, M. Ma, J. Li, Z. Fan and M. Shi, "Surface plasmon induced polarization filter based on Au wires and liquid crystal infiltrated photonic crystal fibers," *Plasmonics,* vol. 11, no. 2, pp. 459-464, 2016.

[161] M. F. O. Hameed, A. M. Heikal, B. M. Younis, M. Abdelrazzak and S. S. A. Obayya, "Ultra-high tunable

liquid crystal-plasmonic photonic crystal fiber polarization filter," *Optics Express,* vol. 23, no. 6, pp. 7007-7020, 2015.

[162] Q. Liu, S. Li, J. Li, C. Dou, X. Wang, G. Wang and M. Shi, "Tunable fiber polarization filter by filling different index liquids and gold wire into photonic crystal fiber," *IEEE Journal of Lightware Technology,* vol. 34, no. 10, pp. 2484 - 2490, 2016.

[163] W. Zhang, S. Li, A. G.-W., Z.-K. Fan and Y.-J. Bao, "Polarization filter characteristics of photonic crystal fibers with square lattice and selectively filled gold wires," *Applied Optics,* vol. 53, no. 11, pp. 2441-2445, 2014.

[164] G. An, S. Li, X. Yan, Z. Yuan and X. Zhang, "High-birefringence photonic crystal fiber polarization filter based on surface plasmon resonance," *Applied Optics,* vol. 55, no. 6, pp. 1262-1266, 2016.

[165] L.-H. Jiang, Y. Zheng, J.-J. Yang, L.-T. Hou, J.-Y. Peng and X.-T. Zhang, "Design of an ultrashort single-polarization wavelength splitter based on gold-filled square-lattice photonic crystal fiber," *Optical and Quantum Electronics,* vol. 48, p. 409, 2016.

[166] L. Jiang, Y. Zheng, J. Yang, L. Hou, Z. Li and X. Zhao, "An Ultra-broadband Single Polarization Filter Based on Plasmonic Photonic Crystal Fiber with a Liquid Crystal Core," *Plasmonics,* pp. 1-7, 2016.

[167] A. M. Heikal, F. F. K. Hussain, M. F. O. Hameed and S. S. A. Obayya, "Efficient polarization filter design based on plasmonic photonic crystal fiber," *Journal of Lightwave Technology,* vol. 33, no. 13, pp. 2868 - 2875, 2015.

[168] S. Zhang, X. Yu, Y. Zhang, P. Shum, Y. Zhang, L. Xia and D. Liu, "Theoretical Study of Dual-Core Photonic Crystal Fibers With Metal Wire," *IEEE Photonics Journal,* vol. 4, no. 4, pp. 1178-1187, 2012.

[169] P. Li and J. Zhao, "Polarization-dependent coupling in gold-filled dual-core photonic crystal fibers," *Optics Express,* vol. 21, no. 5, pp. 5232-5238, 2013.

[170] B. Sun, M.-Y. Chen, J. Zhou and Y.-K. Zhang, "Surface plasmon induced polarization splitting based on dual core photonic crystal fiber with metal wire," *Plasmonics,* vol. 8, no. 2, pp. 1253-1258, 2013.

[171] B. Sun, M.-Y. Chen, Y.-K. Zhang and J. Zhou, "Polarization-dependent coupling characteristics of metal-wire filled dual-core photonic crystal fiber," *Optical and Quantum Electronics,* vol. 47, no. 2, pp. 441-451, 2015.

[172] A. Khaleque, E. G. Mironov and H. T. Hattori, "Analysis of the properties of a dual-core plasmonic photonic crystal fiber polarization splitter," *Applied Physics B,* vol. 121, pp. 523-532, 2015.

[173] A. Khaleque and H. T. Hattori, "Ultra-broadband and compact polarization splitter based on gold filled dual-core photonic crystal fiber," *Journal of Applied Physics,* vol. 118, no. 14, p. 143101, 2015.

[174] Z. Fan, S. Li, Q. Liu, H. Chen and X. Wang, "Plasmonic broadband polarization splitter based on dual-core photonic crystal fiber with elliptical metallic nanowires," *Plasmonics,* pp. 1-8, 2016.

[175] Q. Liu, S. Li, Z.-K. Fan, W. Zhang, H. Li, J.-C. Zi and G.-W. An, "Numerical analysis of ultrabroadband polarization splitter based on gold-filled dual-core photonic crystal fiber," *Optics Communications,* vol. 334, pp. 46-50, 2015.

[176] L. Jiang, Y. Zheng, L. Hou, K. Zheng, J. Peng and X. Zhao, "An ultrabroadband polarization splitter based on square-lattice dual-core photonic crystal fiber with a gold wire," *Optics Communications,* vol. 351, pp. 50-56, 2015.

[177] M. F. O. Hameed, R. T. Balat, A. M. Heikal, M. M. Abo-Elkhier, M. I. A. E. Maaty and S. S. A. Obayya, "Polarization-independent surface plasmon liquid crystal photonic crystal multiplexer–demultiplexer," *IEEE Photonics Journal,* vol. 7, no. 5, p. 4801110, 2015.

[178] L. Chen, W. Zhang, Q. Zhou, Y. Liu, J. Sieg, Y. Zhang, L. Wang, B. Wang and T. Yan, "Polarization rotator based on hybrid plasmonics photonic crystal fiber," *IEEE Photonics Technology Letters,* vol. 26, no. 22, pp. 2291-2294, 2014.

[179] C. Dou, X. Jing, S. Li, Q. Liu and J. Bian, "A photonic crystal fiber polarized filter at 1.55 μm based on surface plasmon resonance," *Plasmonics,* vol. 11, no. 4, pp. 1163-1168, 2015.

[180] X. Hao, S. Li, X. Yan, X. Zhang, G. An, H. Wang, Y. Shao and Z. Han, "Photonic crystal fibre polarization filter with round lattice based on surface plasmon resonance," *Journal of Modern Optics,* pp. 1-5, 2016.

[181] G. Wang, S. Li, G. An, X. Wang and Y. Zhao, "Design of a polarization filtering photonic crystal fiber with a big gold-coated air hole," *Optical and Quantum Electronics,* vol. 48, p. 457, 2016.

[182] L. Jiang, Y. Zheng, L. Hou, K. Zheng and J. Peng, "Surface plasmon induced polarization filter of the gold-coated photonic crystal fiber with a liquid core," *Optical Fiber Technology,* vol. 23, pp. 42-47, 2015.

[183] J. Xue, S. Li, Y. Xiao, W. Qin, X. Xin and X. Zhu, "Polarization filter characters of the gold-coated and the liquid filled photonic crystal fiber based on surface plasmon resonance," *Optics Express,* vol. 21, no. 11, pp. 13733-13740, 2013.

[184] X. Wang, S. Li, H. Chen, Q. Liu, G. Wang and Y. Zhao, "Compatibility of Temperature Sensor and Polarization Filter Based on Au Film and Glycerin Selectively Infilling Photonic Crystal Fibers,"

Plasmonics, vol. 11, no. 5, pp. 1265-1271, 2016.

[185] Q. Liu, S. Li and H. Chen, "Two kinds of polarization filter based on photonic crystal fiber with nanoscale gold film," *IEEE Photonics Journal,* vol. 7, no. 1, p. 2700210, 2015.

[186] G. Wang, S. Li, X. Wang, Y. Zhao, Q. Liu, J. Zi, H. Li and H. Chen, "A Kind of Broadband Polarization Filter Based on Photonic Crystal Fiber with Nanoscale Gold Film," *Plasmonics,* pp. 1-6, 2016.

[187] Y. Han, L. Xia, Y.-T. Zhang and W. Li, "Ultra-broad band single-polarization single-mode photonic crystal fiber based on the zero-order surface plasmon polariton mode," *Optics Communications ,* vol. 345, pp. 141-148, 2015.

[188] H. Chen, S. Li, M. Ma, Z. Fan and Y. Wu, "Ultrabroad bandwidth polarization filter based on D-shaped photonic crystal fibers with gold film," *Plasmonics,* vol. 10, no. 5, pp. 1239-1242, 2015.

[189] H. Chen, S. Li, G. An, J. Li, Z. Fan and Y. Han, "Polarization splitter based on D-Shaped dual-core photonic crystal fibers with gold film," *Plasmonics,* vol. 10, no. 1, pp. 57-61, 2015.

[190] Z. Fan, S. Li, Q. Liu, J. Li and Y. Xie, "Plasmonic polarization beam splitter based on dual-core photonic crystal fiber," *Plasmonics,* vol. 10, no. 6, pp. 1283-1289, 2015.

[191] L. Chen, W. Zhang, Z. Zhang, Y. Liu, J. Sieg, L. Zhang, Q. Zhou, L. Wang, B. Wang and T. Yan, "Design for a single-polarization photonic crystal fiber wavelength splitter based on hybrid-surface plasmon resonance," *IEEE Photonics Journal,* vol. 6, no. 4, p. 2200909, 2014.

[192] Q. Liu, S. Li, J. Li, H. Chen, Z. Fan, G. An, H. Li and J. Zi, "Photonic crystal fiber polarization filter based on coupling between core mode and SPP mode," *Plasmonics,* vol. 11, no. 3, p. 857–863, 2016.

[193] G. Wang, S. Li, G. An, X. Wang, Y. Zhao and W. Zhang, "Design of a polarized filtering photonic-crystal fiber with gold-coated air holes," *Applied Optics,* vol. 54, no. 30, pp. 8817-8820, 2015.

[194] J. Zi, S. Li, W. Zhang and G. An, "Polarization filter characteristics of square lattice photonic crystal fiber with a large diameter gold-coated air hole," *Plasmonics,* vol. 10, no. 6, p. 1499–1504, 2015.

[195] J. Zi, S. Li, H. Chen, J. Li and H. Li, "Photonic crystal fiber polarization filter based on surface plasmon polaritons," *Plasmonics,* vol. 11, no. 1, pp. 65-69, 2016.

[196] Q. Liu, S. Li, H. Li, J. Zi, W. Zhang, Z. Fan, G. An and Y. Bao, "Broadband single-polarization photonic crystal fiber based on surface plasmon resonance for polarization filter," *Plasmonics,* vol. 10, no. 4, pp. 931-939, 2015.

[197] A. Khaleque and H. T. Hattori, "Polarizer based upon a plasmonic resonant thin layer on a squeezed photonic crystal fiber," *Applied Optics,* vol. 54, no. 9, pp. 2543-2549, 2015.

[198] H. Li, S. Li, H. Chen, J. Li, G. An and J. Zi, "A Polarization Filter Based on Photonic Crystal Fiber with Asymmetry Around Gold-Coated Holes," *Plasmonics,* vol. 11, no. 1, pp. 103-108, 2016.

[199] D. Poudereux, M. Caño-García, J. F. Algorri, B. García-Cámara, J. M. Sánchez-Pena, X. Quintana, M. A. Geday and J. M. Otón, "Thermally tunable polarization by nanoparticle plasmonic resonance in photonic crystal fibers," *Optics Express,* vol. 23, no. 22, pp. 28935-28944, 2015.

[200] S. Bose, R. Chattopadhyay, S. Roy and S. K. Bhadra, "Study of nonlinear dynamics in silver-nanoparticle-doped photonic crystal fiber," *Journal of Optical Society of America B,* vol. 33, no. 6, pp. 1014-1021, 2016.

[201] M. Sadeghi, V. Ahmadi and M. Ebnali-Heidari, "Metal-coated silicon nanowire embedded plasmonic photonic crystal fiber: Kerr nonlinearity and two-photon absorption," *Plasmonics,* 2016.

[202] A. Tuniz, B. T. Kuhlmey, P. Y. Chen and S. C. Fleming, "Weaving the invisible thread: design of an optically invisible metamaterial fibre," *Optics Express,* vol. 18, no. 17, pp. 18095-18105, 2010.

[203] H. Tyagi, H. W. Lee, P. Uebel, M. A. Schmidt, N. Joly, M. Scharrer and P. S. J. Russell, "Plasmon resonances on gold nanowires directly drawn in a step-index fiber," *Optics Letters,* vol. 35, no. 15, pp. 2573-2575, 2010.

Although as thin as human hairs, optical fibers have revolutionized our life in many ways. It is exciting to use optical fibers to manipulate light and create solutions to address real-life problems.

Biography

 Dr. Dora Juan Juan Hu

Dora received her B.Eng (1st Hon.) and Ph.D degree from the school of Electrical and Electronic Engineering, Nanyang Technological University, Singapore in 2004 and 2010 respectively. She joined the RF & Optical Department, Institute for Infocomm Research, Agency for Science, Technology and Research (A*STAR), Singapore from 2009 to 2012 to develop novel fiber devices for sensor applications. In 2012 she received A*STAR post-doctoral fellowship (2012-2014). In 2012 she joined the Wellman Center for Photomedicine, Massachusetts General Hospital, Boston, USA as a research fellow and worked on novel photonic technologies for endoscopic diagnosis. Dora joined the Femtosecond Optics Group, Imperial College London in August 2013 and worked on visible and mid-infrared fiber lasers. She is now with the Smart Energy and Environment Cluster, Institute for Infocomm Research, Agency for Science, Technology and Research (A*STAR), Singapore and working on developing photonic solutions for smart infrastructure and healthcare industry.

H.P. Ho received his BEng and PhD in Electrical and Electronic Engineering from the University of Nottingham in 1986 and 1990 respectively. Currently a professor in the Department of Electronic Engineering, The Chinese University of Hong Kong (CUHK), he has held positions as Associate Dean of Engineering, CUHK, Assistant Professor in the Department of Physics and Materials Science, City University of Hong Kong, and Senior Process Engineer for semiconductor laser fabrication in Hewlett-Packard. Started as a compound semiconductor materials scientist, his current academic interests focus at nano-sized semiconductor materials for photonic and sensor applications, optical instrumentation, surface plasmon resonance biosensors, lab-on-a-chip and biophotonics. He has published over 300 peer-reviewed articles, 16 Chinese and 6 US patents. He is a Fellow of SPIE and HKIE, and a senior member of IEEE.